FACULTY OF SCIENCE
UNIVERSITY OF COPENHAGEN

The Shockley Model for Topological Insulators

Peter Røhr Beresford Tunstall

Bachelor's thesis in Physics

Advisor: Jens Paaske

Niels Bohr Institute

University of Copenhagen

Date: June 14, 2016

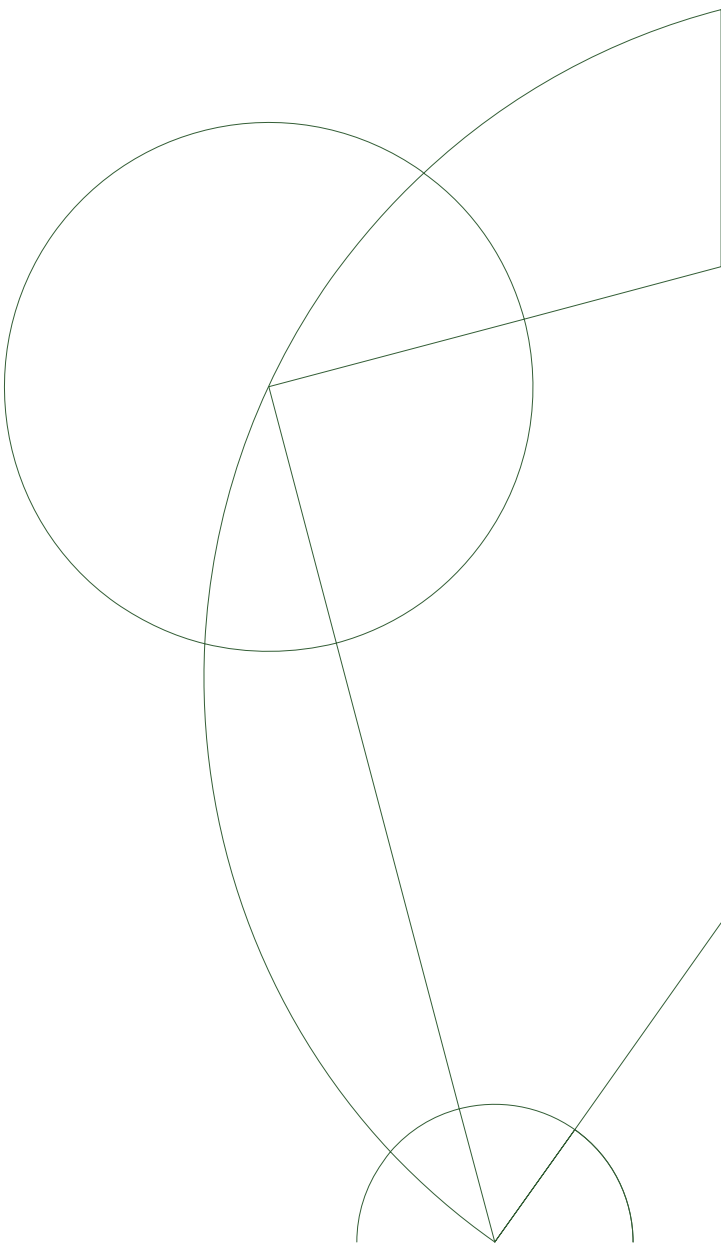

Abstract

In this thesis, the Shockley model for topological insulators is used to analyze the properties of localized edge states in a 1D system. This was done by deriving analytical solutions to bulk- and boundary states, and comparing these with numerical calculations. The relation between the existence of zero-energy edge states and topological properties of the bulk Hamiltonian is described, and finite size effects are characterized. The 1D model is generalized to 3D, where spin is now taken into consideration by adding a Rasha spin-orbit coupling term. The energy spectrum and wavefunctions are derived, and as an example, the model is used for a diamond lattice structure. Lastly, the concept of topological invariants is illustrated and its usage for determining which materials can be topological insulators is discussed.

Contents

List of Figures

1 Introduction

In the last few decades there has been an important advance in condensed matter physics, which is the discovery of topological quantum systems. One of these systems is the so-called topological insulator (TI), and in these there have been observations of states that possess extraordinary properties. They can, for example, accomodate states that can only live on the surface of the material, which show immunity to disorder, and have spin locked perpendicular to the momentum[1]. As we will see in this thesis, such states are characteristic of the topological state of matter, and will be described in detail.

Topology is a mathematical branch concerned with the properties of geometrical objects that are preserved under continuous deformation. In ordinary language, these are the attributes of a shape that we cannot change by only squeezing or expanding, if we are not allowed to tear or punture the object. An orange is therefore topologically equivalent to a banana, but not to a doughnut, as the first cannot be deformed continuously to make a hole in the middle. The hole in this case, plays the role of a *topological invariant*. Similarly, topological insulators have properties that are preserved, even if we change the parameters in the Hamiltonian continously. A change in a topological invariant is evidence of a topological phase transition. The difference between a topological phase transition and a normal phase transitions will be described in subsequent sections. The first sign of topology in condensed matter physics was found in 2D integer quantum hall systems, where the Hall conductance only takes integer multiples of a conduction "quanta", i.e. $\sigma_{xy} = \nu\frac{e^2}{h}$, where ν is an integer. In 1982 it was shown that this integer (called the filling factor) was a topological invariant [2]. This invariant has been shown experimentally to be an integer accurate to a 10^{-9} precision, and is an example of a type $\mathbb{Z}$ index (which can be any positive integer), but topological insulators can also be type $\mathbb{Z}_2$ (which can only be 0 or 1, topologically trivial or non-trivial). The quantum hall effect (QHE) occurs in systems in a magnetic field and only in 2D, but in topological insulators, edge states can exist without an external field. It is then called the *quantum spin hall effect* (QSHE), because of the spin-momentum locking and can exist even in 3D systems.

The topological insulators are formed by elements having high atomic number Z, as relativistic effects of the electrons are more prominent in heavier elements, and they can play the role of the magnetic field. The bulk material is an insulator, in which valence electrons are prohibited from conduction by a band gap. Because of the *Bulk-boundary correspondance* a topological state has associated edge/surface states, which have dispersions going from the valence band to the conduction band, hence the name *gapless*. These are protected from disorder by time-reversal symmetry, but it is possible to create a gap in the dispersion of the edge states. For example, one can create a gap by introducing a superconductor to a surface, where Majorana fermions can exist. These have the property of being their own anti-particles, and are of great interest in the development of quantum computers[1].
In this thesis I will first describe a simple 1D model, which later will be generalized to 3D, and the focus will be on the characteristics of the edge states, and the criteria for their existence. Surprisingly, this can all be described using the good old band theory and ordinary quantum mechanics, so let us get started.

2 1D Shockley model

2.1 The Hamiltonian for the system

In this section the 1-dimensional Shockley model will be treated (as in [3]), and the criteria for the existence of edge-states will be derived. I will first note that all figures in this thesis are self-made unless otherwise stated, , and all plots and calculations are made with Mathematica^{TM}. Let us consider a linear chain of atoms, with two different atoms in the unit cell, A and B, depicted in figure 1. Interactions between the electrons are neglected, and to begin with the spin degree of freedom will be abscent from consideration. For simplicity, the wavenumber k will be a dimensionless quantity throughout the analytical calculations.

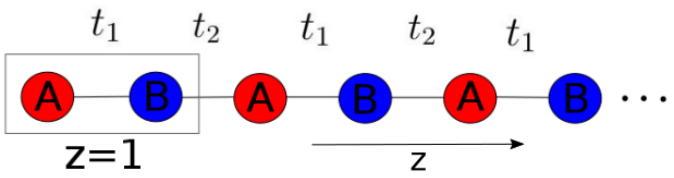

Figure 1: Sketch of the 1D chain of atoms in consideration. The integer unit cell coordinate is denoted by z, and the intracell and intercell hopping amplitudes are denoted by t_1 and t_2 respectively. The grey box depicts the unit cell

The chain of atoms are connected by alternating tight-binding hopping amplitudes, t_1 and t_2. These are a measure for the bond energy between two adjacent atoms, determined by inter-atomic matrix elements. If $t \to 0$, it is impossible for an electron to hop into neighbouring sites. If the hopping term exists between two atoms ($t > 0$), electrons will stay on both of them, thereby lowering their kinetic energy. These hopping amplitudes can be staggered, i.e. ($t_1 \neq t_2$). To find the eigenstates of the system, and the energy spectrum, I will analyze the corresponding Hamiltonian for the system [3]. This can be written in a second quantized form as

$$\mathcal{H} = \sum_z \Psi^\dagger(z) \left[\mathcal{U}\Psi(z) + \mathcal{V}\Psi(z-1) + \mathcal{V}^\dagger\Psi(z+1)\right] \tag{1}$$

$$\mathcal{U} = \begin{pmatrix} 0 & t_1^* \\ t_1 & 0 \end{pmatrix} \qquad \mathcal{V} = \begin{pmatrix} 0 & t_2^* \\ 0 & 0 \end{pmatrix}$$

Here t_1 (intracell) and t_2 (intercell) are the aforementioned tunneling amplitudes, z is the unit cell coordinate and $\Psi(z)$ is the spinor

$$\Psi(z) = \begin{pmatrix} \psi_a(z) \\ \psi_b(z) \end{pmatrix}$$

Where $\psi_a(z)$ and $\psi_b(z)$ are the wavefunctions on the A or B sublattice respectively. In other words, $\Psi(z)$ is the unit cell wavefunction, which contains the sublattice space of A and B. The operator $\mathcal{U}$ accounts for the intracell hopping, as it only contains t_1 and acts on the same cell (only a $\Psi(z)^\dagger\mathcal{U}\Psi(z)$ term occurs in the Hamiltonian). Conversely, the operator $\mathcal{V}$ only contains t_2 and acts on both adjacent cells (it couples to $\Psi(z-1)$ and $\Psi(z+1)$).

2.2 Energy spectrum and eigenstates

Like all solid-state systems, our chain of atoms can be divided into two regimes, the *bulk* and the *boundary*. Firstly, the characteristics of the bulk will be described. To solve the Hamiltonian in Eq. (1), it is a good idea to Fourier transform (which is always a good idea when dealing with nearest neighbour coupling). We assume periodic boundary conditions for the bulk, for simplicity. The Fourier transformation then takes the form

$$\Psi(z) = \int_0^{2\pi} \frac{dk}{2\pi} e^{ikz} \Psi(k) \tag{2}$$

Where our wavefunctions will now be a function of k, i.e. the crystal momentum. Crystal momentum is like a wave envelope that describes how the function varies from one unit cell to the next. Inserting this in Eq. (1) collapses the sum over z, and one obtains

$$\mathcal{H} = \int_0^{2\pi} \frac{dk}{2\pi} \left(\Psi^\dagger(k) \left[\mathcal{U} + \mathcal{V} e^{-ik} + \mathcal{V}^\dagger e^{ik} \right] \Psi(k) \right) = \int_0^{2\pi} \frac{dk}{2\pi} \Psi^\dagger(k) \mathcal{H}(k) \Psi(k) \tag{3}$$

Where $\mathcal{H}(k)$ is the *bulk momentum space Hamiltonian* for the system, acting on the AB sublattice space. Using the expressions for $\mathcal{U}$ and $\mathcal{V}$, it writes

$$\mathcal{H}(k) = \begin{pmatrix} 0 & t^*(k) \\ t(k) & 0 \end{pmatrix}, \qquad t(k) \equiv t_1 + t_2 e^{ik} = t_1 + t_2 q \tag{4}$$

Where $q = e^{ik}$. The Schrödinger equation for this Hamiltonian thus becomes

$$\mathcal{H}(k)\Psi(k) = E(k)\Psi(k) \qquad \Leftrightarrow \qquad \begin{pmatrix} 0 & t^*(k) \\ t(k) & 0 \end{pmatrix} \begin{pmatrix} \psi_a(k) \\ \psi_b(k) \end{pmatrix} = E(k) \begin{pmatrix} \psi_a(k) \\ \psi_b(k) \end{pmatrix} \tag{5}$$

Solving this eigenvalue problem is straight-forward, and if t_1 and t_2 are assumed real, the energy spectrum and eigenstates are

$$E(k) = \pm |t(k)| = \pm \sqrt{t_1^2 + t_2^2 + 2t_1 t_2 \cos k} \qquad \Psi(k) = \frac{1}{\sqrt{2}} \begin{pmatrix} e^{i \arg[t(k)]} \\ \pm 1 \end{pmatrix} \tag{6}$$

Which corresponds to two particle-hole symmetric energy bands plotted in figure 2. Interestingly, one notices that the bulk eigenstates have equal probability of living on either sublattice ($\langle \psi_a | \psi_a \rangle = \langle \psi_b | \psi_b \rangle = \frac{1}{2}$), and it does not depend on the hopping amplitudes.

2.3 Real space bulk eigenstates - analytical and numerical

To find the real space eigenstates for a finite system, one needs to impose the corresponding boundary conditions. In the following, I will work with the atomic coordinate x instead of the unit cell coordinate z. Because of inversion symmetry $E_k = E_{-k}$, so the general solution inside the crystal will be a superposition of the form [4]

$$\Psi_\pm(x) = A\Psi_\pm(k) e^{ikx} + B\Psi_\pm(-k) e^{-ikx} \qquad \Psi_\pm(0) = \Psi_\pm(N+1) = 0 \tag{7}$$

Where N is the number of sites, and A and B are complex constants to be determined by the boundary conditions.

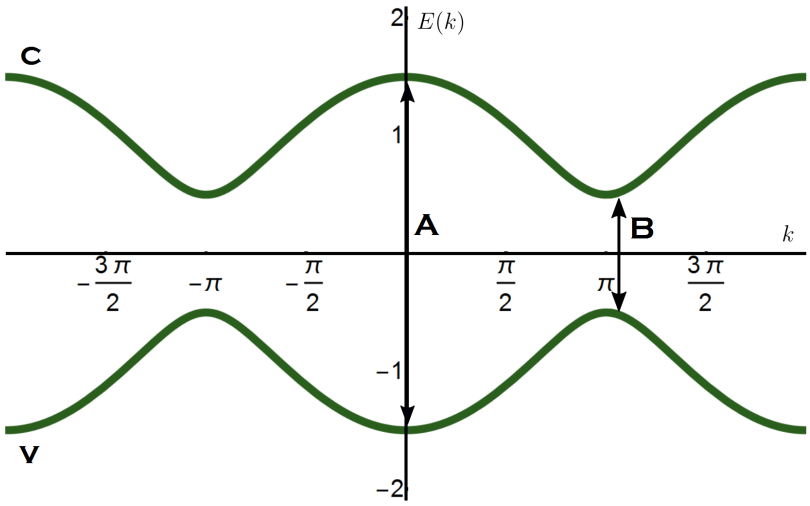

Figure 2: Plot of the symmetric bulk energy spectrum in Eq. (6) for $t_1 = 0.5$ and $t_2 = 1$. In general there will be a non-zero energy gap for staggered hopping amplitudes ($t_1 \neq t_2$), with the size $B = |t_1 - t_2|$, and the maximum distance between the bands is $A = |t_1 + t_2|$. The C-band is the conduction band, and the V-band is the valence band. The latter will be completely filled for $T \to 0$, up to the Fermi energy E_F (in this case at $E_F = 0$), thus describing an insulator.

It should be noted that in this analysis, the lattice constant a is set to unit length. The boundary conditions are made such that the wavefunction vanishes in the fictious sites $x = 0$ and $x = N+1$. From this we get the quantization of the crystal momentum to be $k_l = \frac{\pi}{N+1} l$, and the bulk wavefunctions are found using Eq. (7) and inserting Eq. (6), which gives

$$\Psi_{\pm}(x) = C \begin{pmatrix} \sin(k_l x + \arg\left[t(k_l)\right]) \\ \pm \sin(k_l x) \end{pmatrix}$$

Where $C = \frac{1}{\sqrt{\langle \Psi | \Psi \rangle}}$ is some overall normalization constant determined numerically. The $\pm$ in the B-lattice function in the spinor is associated with $E_{\pm}$. If the energy is negative the two functions are of opposite amplitudes as seen in figure 3, where the analytical solutions are plotted with the numerical calculations (more in Appendix A).

2.4 Edge states

To analyze the edge states, we first introduce a cut in the 1D chain and consider it a half-infinite system for simplicity, as in figure 1. This corresponds to a cut in a t_2-link, so an A atom is exposed on the edge. The wavefunctions are now described with the unit cell coordinate z, and boundary conditions are imposed, such that the wavefunctions vanish at a fictious site $z = 0$ and $z \to +\infty$, i.e.

$$\psi_a(0) = 0, \qquad \psi_b(0) = 0 \tag{8}$$

$$\psi_a(+\infty) = 0, \qquad \psi_b(+\infty) = 0 \tag{9}$$

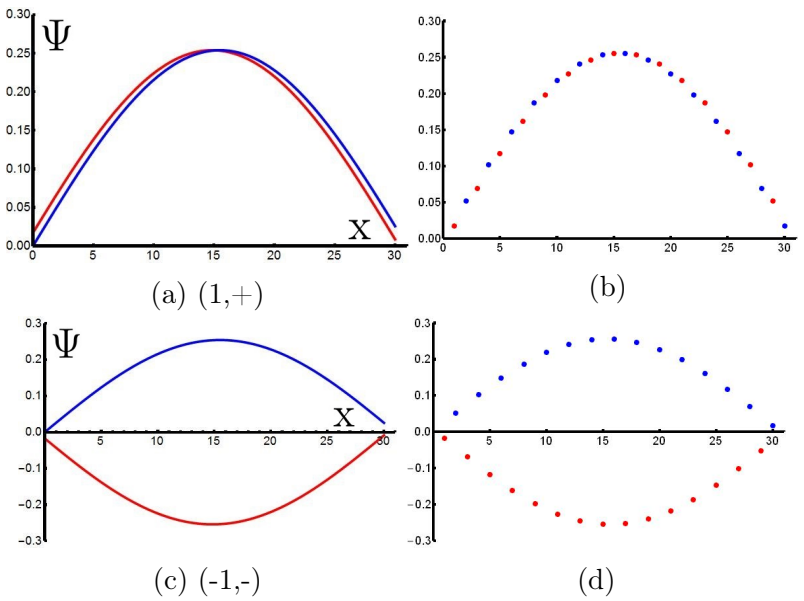

(a) (1,+) (b)

(c) (-1,-) (d)

Figure 3: Plot of the analytical bulk solutions a and c together with the numerical solutions b and d, for $n = 30$ lattice sites. The red colour is sublattice A and the blue is sublattice B. The analytical solutions are denoted with (l,sign(E).). Additional functions can be seen in Appendix E.

Something interesting happens when the hopping amplitudes are of equal strenth $|t_1| = |t_2|$, as there now exist a k_0 such that $E(k_0) = t(k_0) = 0$ from Eq. (6). A zero-energy mode has come into existence! In this particular case $k_0 = \pi$ but in general it is possible to have a zero-enery state for $|t_2| > |t_1|$ as we see in Eq. (4)

$$t(k_0) = t_1 + t_2 e^{ik_0} = t_1 + t_2 q_0 = 0 \Leftrightarrow q_0 = -\frac{t_1}{t_2} \tag{10}$$

This implies that for the zero-energy mode, k_0 is a complex number. This may seem spooky, but it is generally the case that there can exist solutions with complex wavevectors inside the energy gap, and it turns out that these are situated at the surface on a finite sized crystal [5], hence the name edge state. To find the wavefunction for this state we solve the Schrödinger equation in Eq. (5) with $E(k) = 0$. The two equations for the sublattices then decouple, and give

$$t(k)\psi_a(k) = (t_1 + t_2 e^{ik})\psi_a(k) = 0$$
$$t^*(k)\psi_b(k) = (t_1^* + t_2^* e^{-ik})\psi_b(k) = 0$$

Where we seek a non-trivial solution. In real space these equations become (using Eq. (2))

$$t_1\psi_a(z) + t_2\psi_a(z+1) = 0 \tag{11}$$
$$t_1^*\psi_b(z) + t_2^*\psi_b(z-1) = 0 \tag{12}$$

Giving recursion relations for the wavefunctions at different values of z. Now, we can find $\psi_b(z)$ from Eq. (12) by utilizing the first boundary condition in Eq. (8). For $z = 1$ we get

$$t_1^*\psi_b(1) + t_2^*\psi_b(0) = t_1^*\psi_b(1) = 0$$

And $\psi_b(1) = 0$ can be used for the equation for $z = 2$ giving $\psi_b(2) = 0$ and so on. The conclusion is that $\psi_b(z) = 0$. The $z-1$-term is not contained in the equation for $\psi_a(z)$, so this might give something. If we now look at Eq. (11) we get for $z = 1$

$$t_1\psi_a(1) + t_2\psi_a(2) = 0$$

If we set $\psi_a(1) = 1$ we get an equation similar to Eq. (10). We then identify $\psi_a(2) = q_0$, and plug this into the equation for $z = 2$

$$t_1\psi_a(2) + t_2\psi_a(3) = t_1 q_0 + t_2\psi_a(3) = 0 \Leftrightarrow t_1 + t_2\psi_a(3)q_0^{-1} = 0$$

Which again looks like Eq. (10), but now

$$\psi_a(3)q_0^{-1} = q_0 \Leftrightarrow \psi_a(3) = q_0^2$$

And if one continues, the solution for sublattice A becomes $\psi_a(z) = q_0^{z-1} =$ and $\Psi_0(z)$ is thus

$$\Psi_0(z) = C\begin{pmatrix}1\\0\end{pmatrix}q_0^{z-1}, \qquad C = \left(\frac{-t_2^2}{t_1^2 - t_2^2}\right)^{-\frac{1}{2}}, \qquad q_0 = -\frac{t_1}{t_2}, \qquad E_0 = 0 \tag{13}$$

Where the normalization constant is found by $C = \frac{1}{\sqrt{\langle\Psi_0|\Psi_0\rangle}}$. This wavefunction is plotted in figure 4, and we see that it decays exponentially into the bulk, with a penetration depth $\xi = 1/\ln|t_2/t_1|$ (appendix B). We can see how localized it is by calculating the expectation value of z

$$\langle z\rangle = \sum_{z=1}^{\infty} C^2 z\left(q_0^{z-1}\right)^2 = \frac{t_2^2}{t_2^2 - t_1^2}$$

This value grows with increasing t_2, so the edge state becomes more localized for small t_2. Also noted is the fact that there is a divergence at $t_1 = t_2$, i.e. the critical value where the edge state disappears.

2.5 Shockley criterion and the winding number

The wavefunction in Eq. (13) has to satisfy the second boundary condition Eq. (9) as well, which is that $\Psi(z)$ has to vanish at infinity. This only happens if

$$|q_0| = \frac{|t_1|}{|t_2|} < 1 \tag{14}$$

Otherwise we would have runaway solutions. Eq. (14) is also known as the Shockley criterion which states:
In the 1D tight-binding model with alternating tunneling amplitudes, the edge state exists if the bond of the greater magnitude is broken at the boundary.[3]

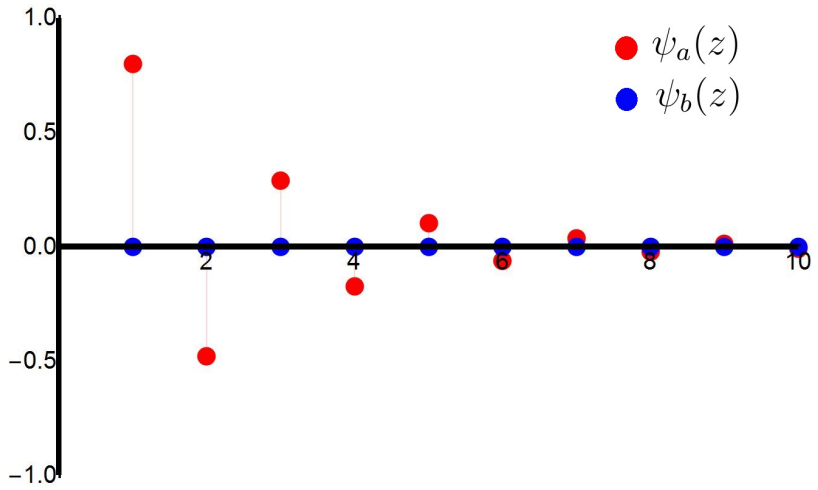

Figure 4: Plot of the wavefunction for the edge state in Eq. (13) on both sublattices, as a function of the unit cell coordinate z for the first 10 unit cells. Here $t_1 = 0.6$ and $t_2 = 1$, and the penetration depth is $\xi = 1.96$.

So if we break the t_2 link, the edge state will exist if $|t_2| > |t_1|$ and vice versa. An interesting consequence is that the edge state only lives on the sublattice exposed to the edge. The Shockley criterion can also be stated in terms of a *Winding number*. When k sweeps the Brillouin zone, $t(k)$ defines a contour in the complex plane C (see figure 5f-5j). This is equivalent to the contour of $t(q)$ for $|q| = 1$. As previously mentioned, if this contour contains the origin, i.e. $t(q_0) = 0$ the edge state exists. This can be formulated by the contour integral

$$W = \frac{1}{2\pi i} \oint_C dq \frac{d}{dq} \ln\left[t(q)\right] \tag{15}$$

Which has the property (shown in Appendix C) that if $t(q_0) = 0$ is inside the contour C we get $W = 1$ and if not we get $W = 0$. In other words, if $|t_2| < |t_1|$ the contour cannot "reach" the origin (see figure 5f and 5g) which is required for the existence of the edge states. This is summarized by

$$W = \begin{cases} 0 & \text{No edge state exists } (|t_2| < |t_1|) \\ 1 & \text{Edge state exists } \quad (|t_2| > |t_1|) \end{cases} \tag{16}$$

This winding number can also be expressed using the bulk Hamiltonian eigenfunctions $\Psi(k)$ from Eq. (6), by what is called the *Zak phase* which can be understood in the following way. If the Hamiltonian undergoes an adiabatic evolution, it will change the eigenstates by a phase factor. This phase has a contribution from the time evolution and one from the *Berry phase*. If the variation is cyclical in a parameter (e.g. the first Brillouin zone) this phase can become an observable invariant. The Zak phase is the Berry phase of the first Brillouin zone[6], and is given by

$$\mathcal{Z} = \frac{1}{i} \oint dk \langle \Psi_k | \partial_k \Psi_k \rangle$$

By using the bulk eigenstates in Eq. (6), and denoting $\phi \equiv \arg[t(k)]$ one gets (proved

in [6])

$$\mathcal{Z} = \frac{1}{2i}\oint i\frac{d\phi}{dk}dk = \frac{\Delta\phi}{2} = \begin{cases}\pi & \text{If } t(k) \text{ encloses the origin}\\ 0 & \text{Otherwise}\end{cases}$$

Where $\Delta\phi$ is the variation in ϕ over the Brillouin zone. So we see, the Zak phase is just π times the winding number of $t(k)$ around the origin. The fact that the Zak phase is calculated with the bulk Hamiltonian eigenfunctions, but tells if an edge state exists, is due to what is called the *Bulk-boundary correspondance*, i.e. characteristics of the physics on the edge can be determined by properties of the bulk.

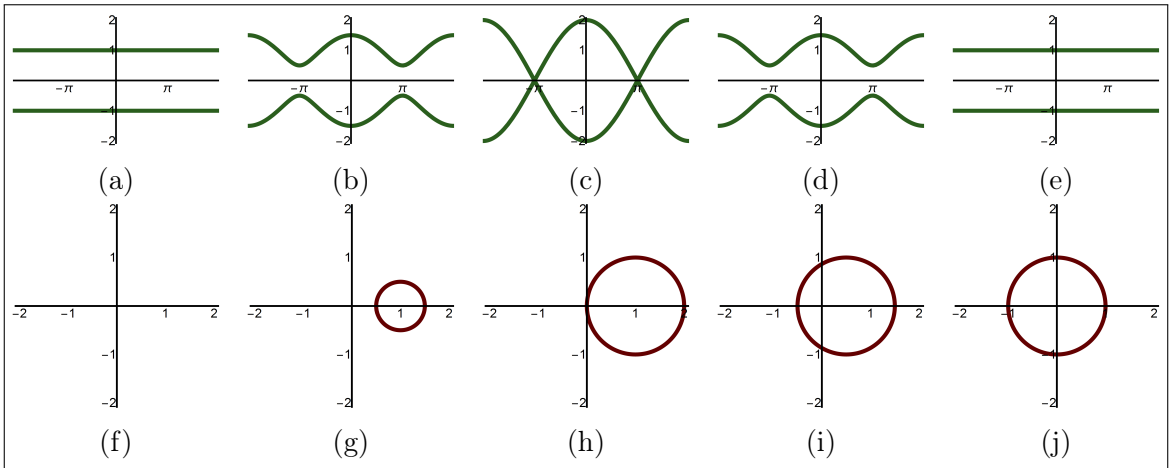

Figure 5: a-e are dispersion relations for five different settings of hopping amplitudes (compare figure 2): (a): $t_1 = 1, t_2 = 0$; (b): $t_1 = 1, t_2 = 0.5$; (c): $t_1 = 1, t_2 = 1$; (d): $t_1 = 0.5, t_2 = 1$; (e): $t_1 = 0, t_2 = 1$. Plotted in f-j are the complex contours of $t(k)$ as the wavenumber k sweeps the Brillouin zone, $k = 0 \to 2\pi$. Interestingly b) and d) look identical, and one could easily be tricked into thinking they were the same insulator, but a topological invariant (the winding numer) distinguishes them.

2.6 Topological phase transitions

Phase transitions can be decribed by Landau Theory, which describes the spontaneous symmetry breaking of a system. For example, a liquid has complete rotational symmetry, while it only has discrete rotational symmetry after the transition to a crystal has occured. But in the case of figure 5, when we vary the parameters through the critical value, no symmetry is broken, so how can a phase transition occur? The transition is said to be a *Topological phase transition*. It is different from our everyday phase transitions, for example the water→ice transition (or in the lives of physicists: paramagnet→ferromagnet or metal→superconductor) which can be called "Landau-like". Here, the transition is not between two distinct symmetries, but between two different topological phases, called the *trivial phase* and the *topological phase* (or *non-trivial phase*) [7]. These two phases can be described by topological invariants, an example of this is the winding number discussed section 2.5.

One can *adiabatically deform* a Hamiltonian, which is to change the parameters without closing the bulk gap, and the new Hamiltonian is then said to be connected to the original. For this to be true the topological invariant cannot change. If the topological invariant changes between two interfaces, a topological transition has occurred, the

bulk gap has at some point been closed, and gapless edge states now exists. This is an example of the Bulk-boundary correspondance. In the 1D case, all Hamiltonians with $|t_2| > |t_1|$ are adiabaticly connected and *non-trivial*, while $|t_2| < |t_1|$ are Hamiltonians in the trivial phase.

2.7 Finite sized system - Numerical solution to edge states

In the analytical calculations in previous sections, a semi-infinte system was considered. Only one edge was exposed, but one can easily imagine that interesting things happen when including the second boundary. The analysis of this was done numerically using the real space tight-binding Hamiltonian in Appendix A. In figure 6, the energy spectrum is shown for different values of the hopping amplitudes t_1 and t_2. We see the expected result, edge states exists for figure 6b with $|t_2| > |t_1|$ and not for 6a. There are two zero energy modes, one for each edge, and as they are degenerate the eigenstates will be in the form of bonding and anti-bonding states shown in Appendix D. As mentioned before, the edge states decay into the bulk with penetration depth $\xi = 1/\ln|t_2/t_1|$, which means that there will be an exponential overlap ($\sim e^{-\frac{\xi}{L}}$ where L is the system length) between the two edge states. This overlap becomes larger for smaller system sizes and will create a gap (*hybridization*), just as in 6c. In figure 16 in Appendix D, the energyspectrum is plotted, as a function of hopping amplitudes, where the same conclusion applies.

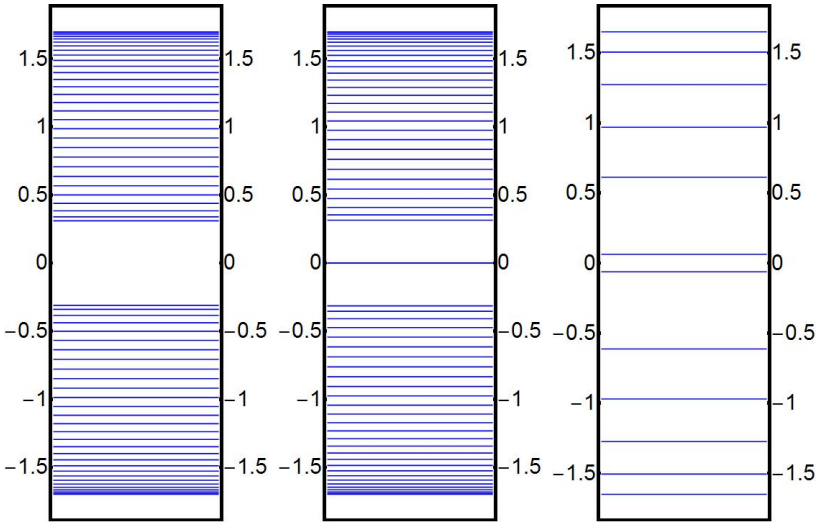

(a) $t_1 = 1$, $t_2 = 0.7$ and $n = 60$ (b) $t_1 = 0.7$, $t_2 = 1$ and $n = 60$ (c) $t_1 = 0.7$, $t_2 = 1$ and $n = 12$

Figure 6: Energyspectra for different values of t_1 and t_2. The Shockley criterion is not sattisfied in a) so we observe no zero energy edge states, while in b) there are two - one for each edge. a) and b) are the same size systems ($n = 60$ lattice sites) while c) is only $n = 12$, so the edge states will hybridize, creating a gap between them.

One weird effect is that even though the constituent particles are electrons, there can exist quasi-particles in the system that carry a fraction of an electronic charge [7]. If we fill the system up with electrons to the Fermi energy $E_F = 0$ in the hybridized case, only the negative energy edge state will be filled. The state hosts 1 electron,

but is placed on either side of the system, so for a sufficiently large system each edge "carry" $\frac{1}{2}e$ charge. This quasiparticle can also be localized on domain walls of the system[7]. This effect is also observed in the biological system Polyacetylene but in this case solitions take the role of the electrons[1].

3 3D Shockley model

The 1D model, discussed in sections 2 can be generalized to 3D by considering the sublattices A and B as two-dimensional atomic layers instead of 1D chains. This is sketched in figure 7, where the layers are perpendicular to the z-direction. In this case, everything in the Hamiltonian in Eq. (34) is now dependent on the in-plane momentum $\mathbf{p} = (p_x, p_y)$. To distinguish between the z-direction and the $xy - plane$, p_z will throughout this thesis be denoted by k. The Hamiltonian includes on-site energy (in this case in-plane), so can be written on the same form as in Appendix F

$$\mathcal{H} = \begin{pmatrix} h(\mathbf{p}) & t^*(k,\mathbf{p}) \\ t(k,\mathbf{p}) & -h(\mathbf{p}) \end{pmatrix} \tag{17}$$

Where the off-diagonal tunneling amplitudes

$$t(k,\mathbf{p}) = t_1(\mathbf{p}) + t_2(\mathbf{p})e^{ik} \tag{18}$$

are now dependent on the in-plane momentum $\mathbf{p}$. The intralayer Hamiltonian is represented by $h(\mathbf{p})$ and is assumed to not depend on the out-of-plane momentum k. This means that there is no coupling between identical sublattices across the unit cells, i.e. no tunneling from A to A or B to B. Similar to the 1D case, a cut of the t_2 link is introduced. For some fixed $\mathbf{p}$, the problem reduces to the 1D case (which will also become apparent later on), where the same conclusions hold, e.g. the Shockley criterion from Eq. (14) still has to be obeyed for there to be gapless edge states. Therefore the $\mathbf{p}$ dependence of $t_1(\mathbf{p})$ and $t_2(\mathbf{p})$ gives a restriction for where in the (p_x, p_y) plane an edge state exists. This can be described by *Vortex lines* in 3D momentum space described in section 3.1.2.

3.1 Rashba spin orbit coupling

When including the spin degree of freedom in the Hamiltonian in Eq. (17), $h(\mathbf{p})$ and $t(k,\mathbf{p})$ become 2×2 matrices, so $\mathcal{H}$ becomes a 4×4 matrix, and the wavefunctions become 4-spinors, including both spin-space and sublattice space. The Hamiltonian can be written in a ingenious form, similar to the 1D case with on-site energies in Appendix F from Eq. (36), with the Pauli vector $\boldsymbol{\tau} = (\tau_x, \tau_y, \tau_z)$. In this case, the dot product consists instead of Kronecker products between the components of $\boldsymbol{\tau}$ and $\mathbf{d}(k,\mathbf{p}) = (\sigma_0 \mathrm{Re}[t(k,\mathbf{p})], \sigma_0 \mathrm{Im}[t(k,\mathbf{p})], h(\mathbf{p}))$. The vector $\mathbf{d}(k,\mathbf{p})$ thus contains the off-diagonal terms $t(k,\mathbf{p})$ and the spin dependent in-plane Hamiltonian $h(\mathbf{p})$

$$\mathcal{H} = \boldsymbol{\tau} \cdot \mathbf{d}(k,\mathbf{p}) = \sum_i \tau_i \otimes d_i(k,\mathbf{p}) \qquad \Psi(k,\mathbf{p}) = \begin{pmatrix} \psi_{a\uparrow} \\ \psi_{a\downarrow} \\ \psi_{b\uparrow} \\ \psi_{b\downarrow} \end{pmatrix} \tag{19}$$

[1] Fractional charge from Topology in Polyacetylene and Graphene - R. Jackiw, MIT

The spin dependence can affect the energies through the so-called *Rashba effect*. This is a momentum dependent spin splitting of bands prevalent in 2D condensed matter systems, when inversion symmetry is broken[2]. The in-plane Hamiltonian $h(\mathbf{p})$ when including the Rashba spin orbit coupling becomes [3]

$$\begin{aligned} h(\mathbf{p}) &= \nu\,(\boldsymbol{\sigma}\times\mathbf{p})\cdot\hat{\mathbf{z}} \\ &= \nu\,[\sigma_x p_y - \sigma_y p_x] \\ &= \nu \begin{pmatrix} 0 & p_y + ip_x \\ p_y - ip_x & 0 \end{pmatrix} \end{aligned}$$

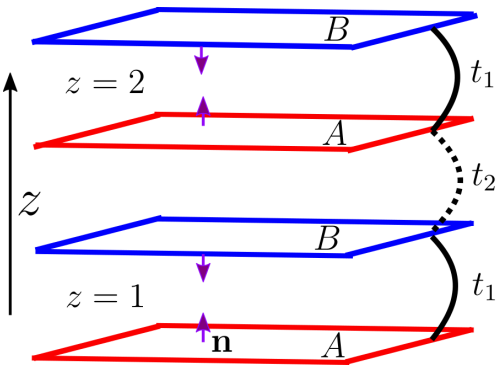

Figure 7: 3D version of the system in figure 1, described by Hamiltonian Eq. 17. The Rashba vector in the spin-orbit coupling is staggered on the sublattices $\mathbf{n} = \pm\hat{z}$.

Where ν is in units of velocity. By assumption, the off-diagonal term $t(k, \mathbf{p})$ is proportional to the unit matrix, i.e. has no spin dependence. In the following, the $(k, \mathbf{p})$ dependence of t will be supressed, for notational convenience. The total Hamiltonian is thus

$$\mathcal{H} = \tau_x \otimes \sigma_0 \mathrm{Re}[t] + \tau_y \otimes \sigma_0 \mathrm{Im}[t] + \tau_z \otimes \nu(\sigma_x p_y - \sigma_y p_x)$$

$$= \begin{pmatrix} 0 & i\ \nu|p|e^{-i\varphi_p} & t^* & 0 \\ -i\ \nu|p|e^{i\varphi_p} & 0 & 0 & t^* \\ t & 0 & 0 & -i\ \nu|p|e^{-i\varphi_p} \\ 0 & t & i\ \nu|p|e^{i\varphi_p} & 0 \end{pmatrix} \tag{20}$$

Where I have rewritten $p_x + ip_y = |p|e^{i\varphi_p}$. The $|p|$ is the magnitude of the in-plane momentum, and φ_p corresponds to the angle from the x-axis to $\mathbf{p}$. The energyspectrum is found in Appendix G to be

$$E_\pm = \pm\sqrt{|t|^2 + \nu^2|p|^2} \tag{21}$$

Which reduces to the 1D energies from Eq. (6) for $p \to 0$. When $t = 0$ the spectrum is gapless, with dispersion

$$E_0 = \pm\nu|p|$$

Surface states with this dispersion exist only if the Shockley criterion is obeyed, i.e. for those p where $|t_2(p)| > |t_1(p)|$. This case is shown in figure 8, where the transparent Dirac cones are dispersions for the surface states. This dispersion is the same linear dispersion as for masless Dirac fermions (the Dirac equation gives surface states living on the interface between systems with negative and positive mass, with dispersion $\epsilon_p = \pm v|p|$ [3]). The spinor eigenfunctions of Eq. (20) are

[2]New perspectives for Rashba spin-orbit coupling - Nature Materials 14, 871-882, 2015 - A. Manchon, H.C. Koo et al.

[3]Topological insulators and the Dirac equation - Shun-Qing Shen, Wen-Yu Shan et al.

$$\Psi^1_\pm = c\begin{pmatrix} \frac{E_\pm}{t} \\ \frac{-i\ \nu|p|e^{i\varphi_p}}{t} \\ 1 \\ 0 \end{pmatrix}, \qquad \Psi^2_\pm = c\begin{pmatrix} \frac{i\ \nu|p|e^{-i\varphi_p}}{t} \\ \frac{E_\pm}{t} \\ 0 \\ 1 \end{pmatrix}, \qquad c = \frac{1}{\sqrt{2\left(1+\frac{\nu^2|p|^2}{|t|^2}\right)}} \tag{22}$$

Which reduces to the 1D spin-degenerate bulk eigenfunctions for $\mathbf{p} \to 0$ (see appendix H).

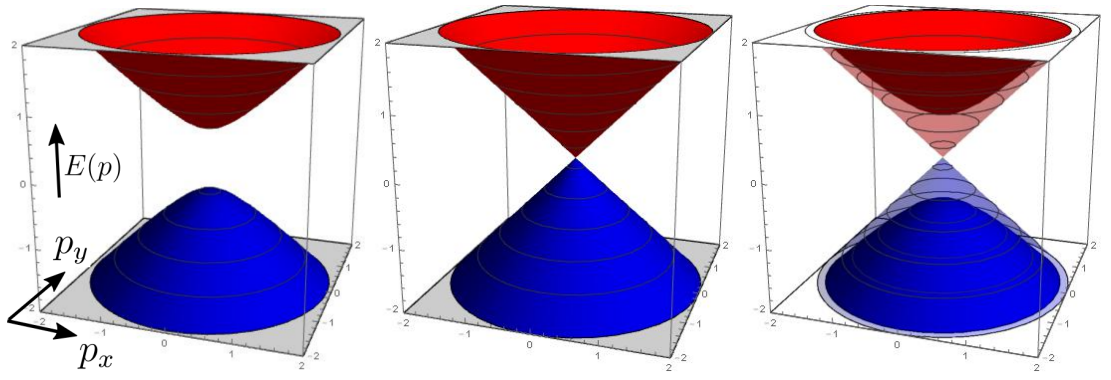

(a) $|t_2| < |t_1|$ (b) $|t_2| = |t_1|$ (c) $|t_2| > |t_1|$

Figure 8: Plots of energyspectra as a function of in-plane momentum, for $k = \pi$. If $|t_2| < |t_1|$ no surface states exists. When $|t_2| = |t_1|$ the Hamiltonian undergoes a topological phase transition, and for $|t_2| > |t_1|$ surface states exist with linear dispersion, illustrated by the transparent Dirac cones. The trivial phase a) could represent vacuum, and the c) phase a TI. At the boundary between these to cases, there will be a closing of the gap which gives rise to the surface states.

3.1.1 Surface state wavefunction

To find the wavefunction for the gapless state, we consider again the cut of a t_2 link, as in figure 7, perpendicular to the $\hat{z}$ direction. The $\hat{x}$ and $\hat{y}$ directions are considered infinite, and will thus have Bloch-wave solutions to the Hamiltonian, due to translational symmetry in the crystal, thus p_x and p_y are good quantum numbers. The interesting part of the total wavefuntion is the z-dependence, so the ansatz is that this will be of the form

$$\Psi^0_{p_y,p_z}(z) = \psi^0_{p_y,p_z} e^{ik_0 z} \tag{23}$$

Where $\psi^0_{p_y,p_z}$ is some z-independent 4-spinor, to be found in the following. The wavenumber k_0 is expected to be imaginary, as to get the exponentially decaying function into the bulk. We find k_0 by solving the equation

$$t(k_0, \mathbf{p}) = t_1(\mathbf{p}) + t_2(\mathbf{p})e^{ik_0} = 0 \Leftrightarrow e^{ik_0} = -\frac{t_1(\mathbf{p})}{t_2(\mathbf{p})}$$

This can then be inserted into Eq. (23), normalized such that $\Psi^0_{p_y,p_z}(1) = \psi^0_{p_y,p_z}$, and denoted $-\frac{t_1(\mathbf{p})}{t_2(\mathbf{p})} \equiv q_0(\mathbf{p})$ similar to the 1D case. We get

$$\Psi^0_{p_y,p_z}(z) = C \cdot \psi^0_{p_y,p_z} \cdot q_0(\mathbf{p})^{z-1}$$

Where C is a normalization constant. As previously mentioned, the 3D case reduces to the 1D case for a fixed value of the in-plane momentum $\mathbf{p}$, and we can see the two cases have the same z-dependence. The surface state is localized on the A-sublattice planes, and exists when the Shockley criterion $|t_2(p)| > |t_1(p)|$ is satisfied [3]. $\psi^0_{p_y,p_z}$ can then be found by analyzing the Schrödinger equation for $\psi_{b\uparrow} = \psi_{b\downarrow} = 0$. This is done in Appendix I. The full beast is then

$$\Psi^0_{p_y,p_z}(z) = C \begin{pmatrix} 1 \\ \mp i e^{i\varphi_p} \\ 0 \\ 0 \end{pmatrix} q_0(\mathbf{p})^{z-1}, \qquad C = \left(\frac{-2t_2(\mathbf{p})^2}{t_1(\mathbf{p})^2 - t_2(\mathbf{p})^2} \right)^{-\frac{1}{2}} \tag{24}$$

Which is very similar to the 1D edge states (see Eq. (13)), where the extra factor 2 in C is due to normalization of the spinor). The wavefunction in Eq. (24) contains the two $\mathbf{p}$-dependent hopping amplitudes $t_1(\mathbf{p})$ and $t_2(\mathbf{p})$, but these are determined by the specific material used. For some $\mathbf{p}$ the z-dependence of this wavefunction is just like the 1D version in Eq. (13), and will thus look like figure 4. The interesting spin structure of $\Psi^0_{p_y,p_z}(z)$ will be analyzed in section 3.1.3.

3.1.2 Vortex lines in 3D momentum space

As we see from Eq. (24), the criterion for existence of surface states might only be satisfied in a certain region of the (p_x, p_y)-plane, in order to sattisfy the boundary conditions. To find this region, we can visualize 3D-momentum space and use the concept of the previously discussed *Winding number* from Eq. (15). We know that the gapless surface states exist when $t(k, \mathbf{p}) = 0$, but $t(k, \mathbf{p})$ is in general a complex number. This gives us two equations $\mathrm{Re}\,[t(k, \mathbf{p})] = 0$, and $\mathrm{Im}\,[t(k, \mathbf{p})] = 0$. In 3D momentum space, two equations will define a line (see figure 9), which will be referred to as a *Vortex line* [3].

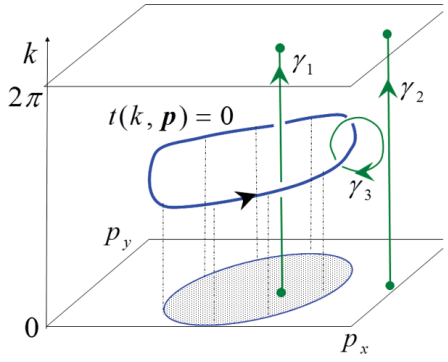

Figure 9: The blue curve corresponds to $t(k, \mathbf{p}) = 0$, while γ_1, γ_2 and γ_3 are contours around which one can calculate the phase winding. The shaded area in the (p_x, p_y)-plane is where the Shockley criterion is satisfied, hence surface states exists in this region. (Picture is from [3])

If we use the integral from Eq. (15), and generalized it to 3D by

$$W(\gamma) = \frac{1}{2\pi i} \oint_\gamma d\mathbf{l} \frac{d}{d\mathbf{l}} \ln[t(k, \mathbf{p})]$$

Evaluated around a closed curve γ, we get the winding number. Here, $\mathbf{l} = (k, \mathbf{p})$ is a parametrisation used for simplicity. For example, the integral around the curve

γ_3 containing the vortex line (figure 9), is $W(\gamma_3) = 1$ just like the 1D case seen in Eq. (16), and Appendix C). The periodicity of the Brillouin zone allows us to define a closed contour γ_1 and γ_2 by varying k for a fixed (p_x, p_y) over the Brillouin zone. These contours can be merged into each other, such that γ_1 and -γ_2 becomes γ_3. We can then conclude

$$W(\gamma_3) = W(\gamma_1) - W(\gamma_2)$$

And from $W(\gamma_{1,2}) \geq 0$ we deduce that $W(\gamma_1) = 1$ and $W(\gamma_2) = 0$. So by Eq. (16), a non-zero winding number is required for the existence of a surface state, and therefore surface states exists in the shaded area in figure 9, i.e. inside the area enclosed by the projection of the vortex line. We will see in subsequent sections that this domain can include Dirac points, and that the number of Dirac points included determines if the TI is in a *weak* phase or a *strong* phase.

3.1.3 Helical surface states

We can now show why the wavefunctions in Eq. (24), have the characteristics of the QSHE. The spin characteristics are calculated in Appendix J, and gives the spin structure shown in figure 10. We see that the spin is locked to the in-plane momentum, hence the name Helical surface states[4]. Electrons travelling in opposite directions will have opposite spin, showing time-reversal symmetry (also discussed in Appendix M). Therefore they are protected from any time-reversal symmetric pertubation[8] as long as it is small enough. One way to understand it is by considering an electron undergoing backscattering. Looking at figure 10, the Fermi surface will be a cross section of this energyspectrum. If an electron reverses its direction of motion, the opposite moving state will already be occupied, so by Pauli's exclusion principle, this cannot happen.

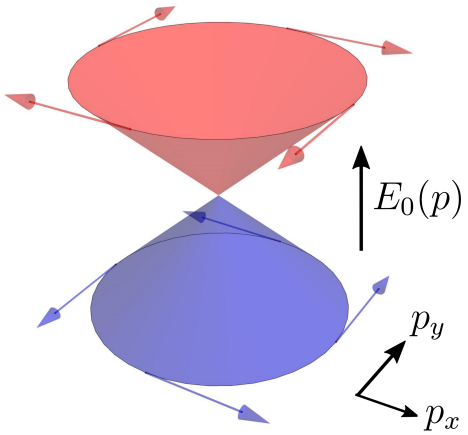

Figure 10: Sketch of the spin structure of the surface state wavefunctions in Eq. (24), superpositioned on the energy spectrum. The starting point of the arrows are the momenta, while the arrow indicates the direction of the spin. These are calculated in Appendix J.

3.2 Shockley model for a diamond lattice

In this section, the model described so far will be used for a particular example, namely for the diamond lattice structure, with a Hamiltonian in the same form as Eq. (17). We consider the crystal structure shown in figure 11, which is a particular orientation of the diamond lattice, and all the relevant vectors used, are depicted as well. The δ_i are in-plane vectors, which can be used to determine the $\mathbf{p}$-dependence of the off-diagonal function $t(k, \mathbf{p})$, which as we have seen, contains most of the information about the surface states.

[4]From particle physics, the *helicity* is the projection of a particles spin along its momentum

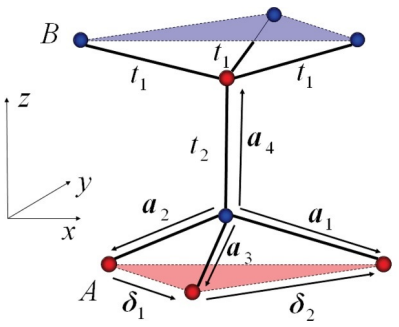

$$\delta_1 = a_3 - a_2 = \left(1/2, -\sqrt{3}/2, 0\right)$$
$$\delta_2 = a_1 - a_3 = \left(1/2, \sqrt{3}/2, 0\right)$$
$$\delta_3 = a_2 - a_1 = (-1, 0, 0)$$

Figure 11: Sketch of the diamond lattice structure, with the hopping amplitudes used in the calculations. The A (red) and B (blue) are sublattice planes. The δ_i are in-plane normalized translation vectors used to determine $t(k, \mathbf{p})$. (Figure is from [3])

The diagonal spin-orbit Hamiltonian $h(\mathbf{p})$ is given by [3]

$$h(\mathbf{p}) = \frac{2\sqrt{2}}{3}\nu_{SO} \sum_{i,j,l=1,2,3} \epsilon_{ijl} \left(\boldsymbol{\sigma} \cdot [a_i \times a_j]\right) \sin(\mathbf{p}\boldsymbol{\delta}_l) \tag{25}$$

Where ν_{SO} is the strength of the spin-orbit interaction, ϵ_{ijl} is the Levi-Civita symbol defined as in Appendix K. The nearest-neighbour vectors a_n, $n = 1, 2, 3$, and calculation of the energy spectrum are shown in Appendix L. As seen before, the energy spectrum of the in-plane Hamiltonian is the same as for the gapless surface states $E_0(\mathbf{p})$

$$\frac{E_0(\mathbf{p})}{\nu_{SO}} = \pm \Big(\frac{32}{9}\Big[\frac{3}{4}\left(\sin^2(\mathbf{p}\boldsymbol{\delta}_1) + \sin^2(\mathbf{p}\boldsymbol{\delta}_2) + \sin^2(\mathbf{p}\boldsymbol{\delta}_3)\right) - \frac{1}{2}\left(\sin(\mathbf{p}\boldsymbol{\delta}_1)\sin(\mathbf{p}\boldsymbol{\delta}_2) + \sin(\mathbf{p}\boldsymbol{\delta}_2)\sin(\mathbf{p}\boldsymbol{\delta}_3) + \sin(\mathbf{p}\boldsymbol{\delta}_3)\sin(\mathbf{p}\boldsymbol{\delta}_1)\right)\Big]\Big)^{\frac{1}{2}} \tag{26}$$

This spectrum is plotted in figure 12. Dirac cones are found at time-reversal-invariant momenta (TRIM) points $p^* \in \{\Gamma, M_1, M_2, M_3\}$ (Appendix L). These points in the Brillouin zone have the property that time-reversal ($\mathbf{p} \to -\mathbf{p}$) brings them to points which can related to the orignal points via reciprocal lattice vectors, i.e. the same crystal momentum ($-\mathbf{p} + \mathbf{G} = \mathbf{p}$). The off-diagonal function $t(k, \mathbf{p})$ is found in [3] to be

$$t(k, \mathbf{p}) = t_1(\mathbf{p}) + t_2 e^{ik}$$
$$t_1(\mathbf{p}) = t_1(1 + e^{-i\mathbf{p}\cdot\boldsymbol{\delta}_1} + e^{i\mathbf{p}\cdot\boldsymbol{\delta}_2})$$

Which describes the tunneling between sublattice planes A and B. Notice that the momentum-dependent function $t_1(\mathbf{p})$ includes the constant tight-binding amplitude t_1, but the two are distinct. It is more convenient to analyze the modulus of this quantity given by

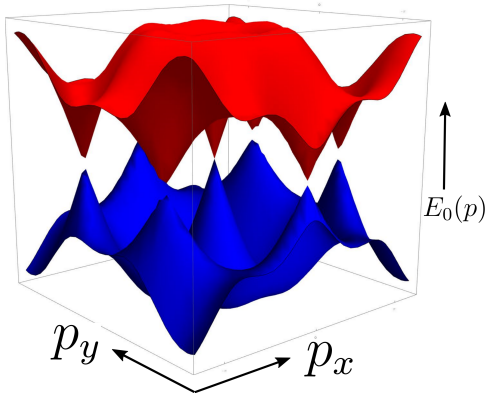

Figure 12: Particle-hole symmetric energy spectrum for the in-plane Hamiltonian in Eq. (25) as a function of in-plane momenta p_x and p_y, for ν_{SO}=1. Notice the Dirac cones at the TRIM points.

$$\frac{|t_1(\mathbf{p})|}{|t_1|} = \frac{\sqrt{t_1(\mathbf{p})^* t_1(\mathbf{p})}}{|t_1|} = \sqrt{3 + 2\cos(\mathbf{p}\boldsymbol{\delta}_1) + 2\cos(\mathbf{p}\boldsymbol{\delta}_2) + 2\cos(\mathbf{p}\boldsymbol{\delta}_3)} \tag{27}$$

In section 3.1.2, it was shown that the criteria for excistence of surface states $t(k, \mathbf{p}) = 0$, defined a vortex line in momentum space, which projection on the (p_x, p_y)-plane defined the area where surface states exists. Given the form of $t(k, \mathbf{p})$ this equation is equivalent to $|t_1(\mathbf{p})| = |t_2|$, which determines the boundary. Consequently, as in previous sections, surface states only exist when the following condition is sattisfied

$$|t_1(\mathbf{p})| < |t_2| \Leftrightarrow \frac{|t_1(\mathbf{p})|}{|t_1|} < \frac{|t_2|}{|t_1|} \equiv \alpha \tag{28}$$

The condition $\frac{|t_1(\mathbf{p})|}{|t_1|} < \alpha$ is shown in figure 13 for various values of α. The Dirac points are shown as well, and whether these are included in the allowed region or not, can determine which phase the TI is in. Whenever an odd amount of Dirac points is included the TI is said to be in a strong topological phase, and for an even number of points, the TI is in the weak phase [9]. In this analysis a cut of the t_2-link was assumed, but if a t_1-link is cut at the boundary, the converse of Eq. (28) is true, i.e. surface states exist for $\frac{|t_1(\mathbf{p})|}{|t_1|} > \alpha$. In figure 13 for this case, the white area is thus where the surface states exist. All these conclusions are summarized in table 1. An even number of Dirac cones can disappear under certain conditions, but for an odd number there will always be at least one Dirac cone. This is the reasoning behind the nomenclature for the phases, and will be discussed again in section 4, where these phases can be attributed to the $\mathbb{Z}_2$ topological indices.

	t_2 cut	t_1 cut	TI phase
$0 < \alpha < 1$	-	$M_{1,2,3}, \Gamma$	Weak
$1 \leq \alpha < 3$	$M_{1,2,3}$	Γ	Strong
$3 \leq \alpha$	$M_{1,2,3}, \Gamma$	-	Weak

Table 1: This table summarizes the conclusions made in this section. Choosing which link is broken at the boundary, one can then determine the included Dirac points for various values of α, and conclude which TI phase the solid is in.

3.3 External magnetic field

In Appendix M the concept of time-reversal symmetry is discussed. By adding an external magnetic field, one can break time-reversal symmetry, and the surface states described in previous sections are no longer symmetry-protected against disorder. If the magnetic field is applied in the $\hat{z}$- direction, and we assume that this will not affect the hopping amplitudes $t_1(p)$ and $t_2(p)$ (i.e. the lattice will not be distorted, which requires large field strengths), the total Hamiltonian can be written as

$$\mathcal{H} = \tau_x \otimes \sigma_0 \mathrm{Re}[t] + \tau_y \otimes \sigma_0 \mathrm{Im}[t] + \tau_z \otimes [\nu(\sigma_x p_y - \sigma_y p_x) + g^* \mu_B B_z \sigma_z]$$

Where g^* is the effective g-factor. By the same method used to obtain Eq. (21), the bulk- and surface spectrum is found to be

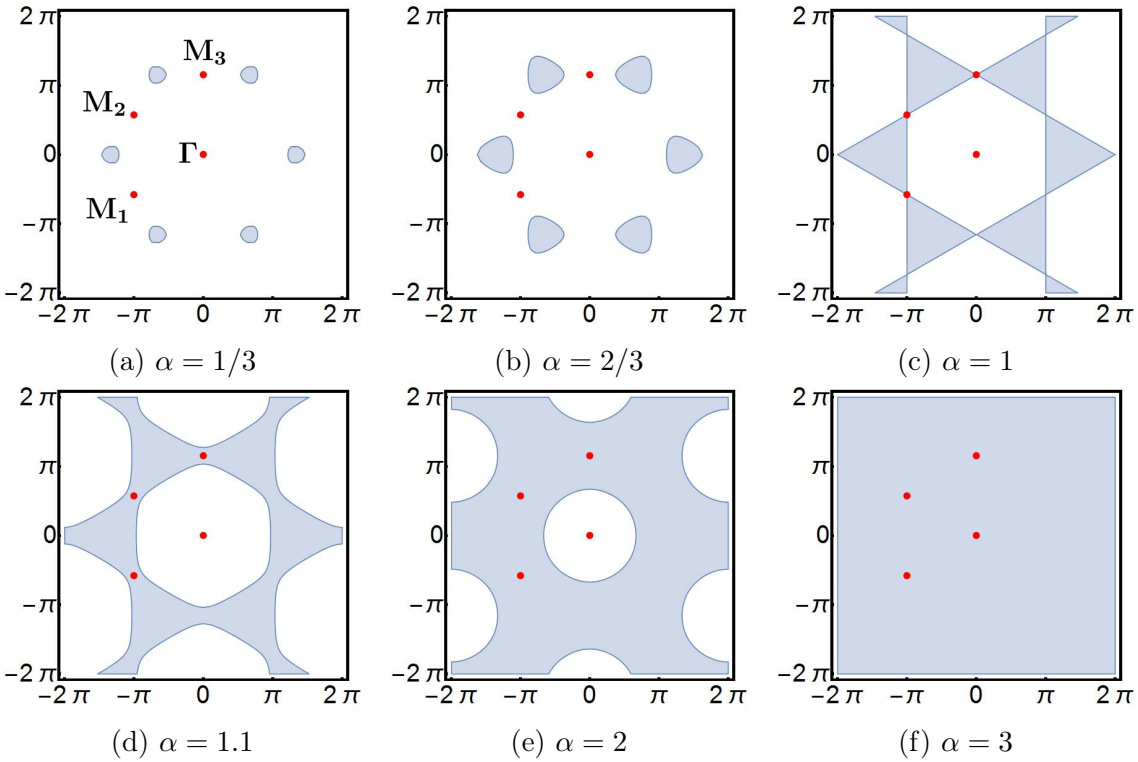

(a) $\alpha = 1/3$ (b) $\alpha = 2/3$ (c) $\alpha = 1$

(d) $\alpha = 1.1$ (e) $\alpha = 2$ (f) $\alpha = 3$

Figure 13: Illustration of the region in the (p_x, p_y)-plane where surface states exists, shown in blue. The red points, marked in a), are the TRIM points of the BZ, and these have associated Dirac cones.

$$E_{\pm} = \pm\sqrt{|t|^2 + \nu^2|p|^2 + (g^*\mu_B B_z)^2}$$
$$E_0 = \pm\sqrt{\nu^2|p|^2 + (g^*\mu_B B_z)^2}$$

Which has opened a gap in the dispersion for the surface states of $\Delta_Z = 2g^*\mu_B B_z$. Where before the surface could be decribed as massless Dirac fermions, now they are massive in the sense that the gap gives a curvature in the dispersion, giving rise to an effective mass $m^* = \hbar^2 \left(\frac{d^2E}{dk^2}\right)^{-1}$. The Quantum Anomalous Hall effect (QAHE) can be realized in this system, which is a version of of the QHE without the need of a strong magnetic fields[5].

4 Topological invariants

As has been mentioned in previous sections, the role of topology in condensed matter systems is expressed in terms of topological invariants. In mathematics, this can for example be expressed in the Gauss-Bonnet theorem [10], relating the integral of the Gaussian curvature of a 2D object embedded in 3D, to its genus (i.e. number of holes). This number is a topological invariant which cannot change under continuous deformation.

[5]Chiral Surface Modes in Three-Dimensional Topological Insulators - Journal of the Physical Society of Japan 85, 053707 (2016) - K. Hattori and H. Okamoto

The topological invariants in condensed matter physics are similar, but describe more abstract spaces. The Gaussian curvature is generalized to a curvature form called the Berry curvature, which can be thought of as a local gauge field connected with the Berry phase, similar to the vector potential in electromagnetism [11]. We have seen that the topological invariants have associated symmetry-protected gapless surface states, which is a demonstration of the Bulk-boundary correspondance. These invariants can be used as a tool to predict what kind of materials that are topological insulators. This section will decribe how to determine the symmetry class of a system, and thus find the corresponding topological classification[9], which topological invariant can the TI be classified with.

The symmetry classes seen in the figure in Appendix N, are defined by the presence/absence of time reversal symmetry Θ (TR), particle-hole symmetry Ξ (PH) (also known as charge conjugation symmetry) and chiral symmetry $\Pi = \Xi\Theta$ (C) (also known as sublattice symmetry), the latter of which is the combination of the first two. These symmetries are present if the bulk momentum space Hamiltonian $\mathcal{H}$ obeys the following transformations [12]

$$\Theta\mathcal{H}(k)\Theta^{-1} = \mathcal{H}(-k) \qquad TR \tag{29}$$

$$\Xi\mathcal{H}(k)\Xi^{-1} = -\mathcal{H}(-k) \qquad PH \tag{30}$$

$$\Pi\mathcal{H}(k)\Pi^{-1} = -\mathcal{H}(k) \qquad C \tag{31}$$

Where one can then determine the symmetry class by finding Θ^2, Ξ^2 and Π^2. Once you have determined the symmetry class of a TI, you can find the topological characteristic in the periodic table of topological systems, shown in Appendix N. No topology means 0, the $\mathbb{Z}$ class is a topological invariant that can take any integer value, and a $\mathbb{Z}_2$ invariant can only take the value 0 or 1 (trivial/non-trivial). An example could be the TKNN[6] invariant from the 2D QHE. In this case, which according to Appendix N is class A (no symmetry), with $d = 2$, the classification is $\mathbb{Z}$, which is precisely the filling factor in the quantized Hall conductance $\sigma_{xy} = \nu\frac{e^2}{h}$, related to the number of filled Landau levels. The QSH phase which we have seen in action in 3D topological insulators, can be differentiated from an ordinary band insulator by the so-called $\mathbb{Z}_2$ topological invariant. For 3D topological insulators there are four $\mathbb{Z}_2$ invariants needed to describe the system, namely $(\nu_0; \nu_1, \nu_2, \nu_3)$ [9]. The ν_0 invariant distinguishes between the weak TI phase ($\nu_0 = 0$) and the strong TI phase ($\nu_0 = 1$), already seen in section 3.2. Here, the spectrum of surface states in the strong phase, included an odd amount of Dirac points, while the weak contained an even amount. So one might ask the question, why does an odd number of Dirac cones imply that the TI is strong? This can be argued from figure 14, which is a plot of the edge state dispersion between two TRIM points Γ_A and Γ_B in a Θ-invariant 2D insulator (Θ is the operation of time-reversal defined in Appendix M).

Depending on the specifics of the Hamiltonian near the edge, one can have edge states within the gap. We know from Kramers theorem that these are two-fold degenerate at the TRIM points, due to $E(k) = E(-k)$. Away from these points, spin-orbit coupling will split the degeneracy into two levels. There are two ways in which states at Γ_A can connect to states at Γ_B. One is depicted in figure 14a, where they connect pairwise,

[6]Named after Thouless-Kohmoto-Nightingale-den Nijs

and the Fermi energy E_F thus crosses an even number of times, or not at all. In this case the bound states can be "pushed" out of the energy gap, by adiabatically changing the Hamiltonian, thus eliminating the edge states. In figure 14b, this cannot be done, and the Fermi energy crosses an odd number of times. Hence, the odd number of crossings is topologically protected thereby describing the strong topological phase [9].

Now that I have described the ν_0 invariant, what about the other three? In the weak phase $\nu_0 = 0$, the system can be thought of as stacked 2D QSH states in the direction of a reciprocal lattice vector given by the three remaining invariants $G_\nu = \sum_i^3 \nu_i b_i$. The (ν_1, ν_2, ν_3) are interpreted as Miller indices, explained in Appendix Q. This analogy is lost for $\nu_0 = 1$, which describes an entirely unique topological phase. The method for finding the $\mathbb{Z}_2$ invariant is described in Appendix O.

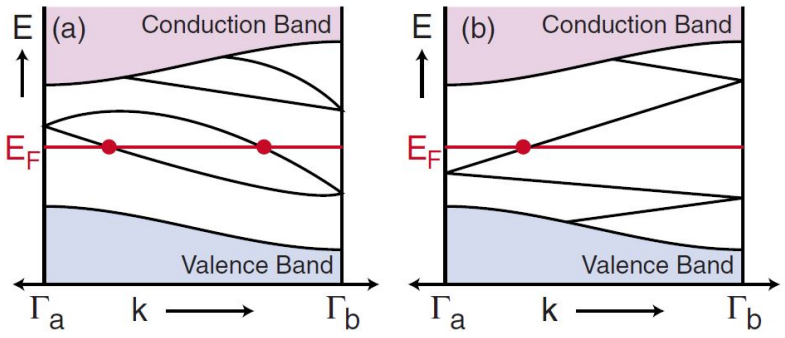

Figure 14: Electron dispersion between TRIM points Γ_A and Γ_B [13]. In *a*) the Fermi energy E_F crosses the edge states an even number of time (weak phase, $\nu_0 = 0$), while in *b*) it crosses an odd number of times (strong phase, $\nu_0 = 1$). (Picture taken from [13]).

As an example, the symmetry class of the 1D Hamiltonian from Eq. (4) is determined in Appendix P. By this method one can determine if a Hamiltonian can be topologically non-trivial, and thus find new materials that are topological insulators. Some TI's were theoretically predicted prior to experimental observation, such as in Graphene ([8]), HgCdTe quantum well structures ([14]), and in $Bi_{1-x}Sb_x$ ([9]). When searching for new materials, a good place to look are materials including atoms with high atomic number Z. This is because heavy atoms have larger relativistic effects to the energyspectrum, necessary to cause band-inversion [13]. For example[7], SO scales with Z^4. In normal insulators (or even vaccum) the conduction band is comprised of s-like electrons and valence band of p-like electrons[13]. Relativistic corrections, like spin-orbit coupling, the Darwin term, the mass-term etc., can be derived by taylor expanding the relativistic Dirac equation in the parameter $\frac{v}{c}$. These can cause the s- and p-bands to swap, so that the filled band consists of p-electrons, and this inverted state can be identified with the topological state. For the bands to invert, there must be a place where they intersect, i.e. the band cross at the boundary where the gapless edge states exists. Most litterature state that the spin-orbit correction is the most important relativistic term for the existence of topological insulators, but more recent

[7] Atomic Physics -Christopher J. Foot - Oxford university press 2005

work states that this is not the case[8].

The most prominent candidate recently discovered is one of the Second generation materials Bi_2Se_3 [15], which has a simple Dirac cone surface spectrum and a large band gap of ≈ 0.3eV (estimate taken from [15] at the Γ point), indicating that it can show topological features even at room temperature! ($\frac{0.3eV}{k_B} = 3480K$). In [3] it is argued that Bi_2Se_3 is indeed a strong TI, which can be decribed with the Shockley model utilized in this thesis. Amazingly, this simple model can describe fairly complex systems, and it will be very exiting to see which topological quantum systems will be found in future work, theoretically or experimentally. Maybe one day a topological insulator at room temperature will even be found in common materials in nature.

5 Conclusion

In this thesis I have described a simple model for topological insulators, called the Shockley model. The main focus has been on the existence of symmetry protected edge/surface states, and how these relate to the topological characteristics. Firstly, the one dimensional system was described by solving the Schrödinger equation for the relevant Hamiltonian, and the analytical solutions were compared to the numerical results. This gave the basis for further analysis, which was the search for zero energy edge states, and the criteria for their existence. Some arguments were given for the topological nature of the system, and finite size effects were discussed. This model was then generalized to three dimensions, where a Rashba spin orbit coupling term was added. The new 3D wavefunctions showed similarities to the 1D case, while also exhibiting spin-momentum locking, and immunity to backscattering by time-reversal symmetry. The criteria for existence of surface states were shown, and as an example, the model could then be used to analyze a diamond lattice structure. Some exotic properties arised when introduced to an external magnetic field, which was briefly discussed. Finally, the concept of *topological invariants* was introduced, and the recipe for finding out which systems can be topological insulators was discussed.

6 Acknowledgements

I would like to thank my advisor Jens Paaske for the inspiration to this project, and for helping whenever a problem ensued. It has been a very exciting time, and the introduction to topics in condensed matter research has been much appreciated. I would like to thank Marieke van Beest and Gorm Ole Steffensen for reading my thesis, and giving valuable feedback. Finally, I would like to thank the CMT group for having me, and to the lunchclub for the everyday entertainment.

7 References

[1] Shun-Qing Shen. The family of topological phases in condensed matter. National Science Review., 2013.

[8] Band inversion mechanism in topological insulators: A guideline for materials design Phys. rev. B 85, 235401 (2012)– Z. Zhu, Y. Cheng et al. -

[2] D. J. Thouless, M. Kohmoto, M. P. Nightingale, and M. den Nijs. Quantized hall conductance in a two-dimensional periodic potential. Phys. Rev., 49(405), 1982.

[3] Sergey S. Perchgova and Victor M. Yakovenko. Schockley model description of surface states in topological insulators. Phys. Rev. B, 86(075304), 2012.

[4] William Shockley. On the surface states associated with a periodic potential. Phys. Rev., 56, 1939.

[5] Charles Kittel. Introduction to solid state physics. Wiley, 2005.

[6] P. Delplace, D. Ullmo, and G. Montambaux. The zak phase and the existence of edge states in graphene. Phys. Rev. B, 84(195452), 2011.

[7] J. K. Asbóth, L. Oroszlány, and A. Pályi. A short Course on Topological Insulators. Springer, 2015.

[8] C. L. Kane and E. J. Mele. Quantum spin hall effect in graphene. Phys. Rev. Letters, 95(226801), 2005.

[9] Liang Fu, C. L. Kane, and E. J. Mele. Topological insulators in three dimensions. Phys. Rev., 98(106803), 2007.

[10] C. L. Kane. Topological Band Theory and the Z2 invariant. Elsevier, 2013.

[11] Andrei Bernevig and Titus Neupert. Topological superconductors and category theory. 2015.

[12] J. C. Y. Teo and C. L. Kane. Topological defects and gapless modes in insulators and superconductors. Phys. Rev. B., 82(115120), 2010.

[13] M. Z. Hasan and C. L. Kane. Colloquium: Topological insulators. RevModPhys, 82(3045), 2010.

[14] B. Andrei Bernevig and Shou-Cheng Zhang. Quantum spin hall effect. Phys. Rev. Letters, 96(106802), 2006.

[15] Haijun Zhang and Chao-Xing Liu et al. Topological insulators in bi2se3, bi2te3 and sb2te3 with a single dirca cone at the surface. Nature Physics, 5(438), 2009.

[16] Liang Fu and C. L. Kane. Topological insulators with inversion symmetry. Phys. Rev. B., 76(045302), 2007.

[17] J. J. Sakurai and J. J. Napolitano. Modern Quantum Mechanics. Pearson, 2014.

[18] K. F. Riley and M. P. Hobson. Essential mathematical methods. Cambridge, 2011.

Appendices

A Real space representation to the 1D Hamiltonian

If one writes out the Hamiltonian from Eq. (1) in a real space basis, e.g. for $N = 3$ unit cells, it reads

$$H = \begin{pmatrix} 0 & t_1^* & 0 & 0 & 0 & 0 \\ t_1 & 0 & t_2 & 0 & 0 & 0 \\ 0 & t_2^* & 0 & t_1^* & 0 & 0 \\ 0 & 0 & t_1 & 0 & t_2 & 0 \\ 0 & 0 & 0 & t_2^* & 0 & t_1^* \\ 0 & 0 & 0 & 0 & t_1 & 0 \end{pmatrix} \tag{32}$$

which has non-zero entries on each side of the diagonal, corresponding to nearest neighbour coupling. The diagonal is zero, because of the abscence of on-site potentials in this model.

B Penetration depth of edge states

The penetration depth ξ is defined at the depth, where the edge state $\psi_a(z)$ has decayed to e^{-1} of its initial value. By plugging in

$$\psi_a(z+\xi) = e^{-1}\psi_a(z) \Leftrightarrow q_0^{z+\xi-1} = e^{-1}q_0^{z-1} \Leftrightarrow q_0^{\xi} = e^{-1}$$
$$\left(-\frac{t_2}{t_1}\right)^{\xi} = e \Leftrightarrow \left|\left(-\frac{t_2}{t_1}\right)^{\xi}\right| = e \Leftrightarrow \left|\frac{t_2}{t_1}\right|^{\xi} = e \Leftrightarrow \xi \ln\left|\frac{t_2}{t_1}\right| = 1 \Leftrightarrow \xi = \frac{1}{\ln\left|\frac{t_2}{t_1}\right|}$$

C The winding number

The winding number in section 2.5 was expressed using the following contour integral

$$W = \frac{1}{2\pi i}\oint_C dq \frac{d}{dq}\ln\left[t(q)\right]$$

If we calculate the integrand using the chain rule, we get

$$W = \frac{1}{2\pi i}\oint_C dq \frac{t'(q)}{t(q)}$$

Which has a pole in $q = q_0$. Therefore, if this pole is not contained in the contour C, as in the cases in figure 5f-5h, we get $W = 0$ according to *Cauchy's theorem*[18]. If the pole is contained in C, as in figure 5i and 5j, we instead use the *residue theorem*. The fact that the integrand is of the form $\frac{g(q)}{h(q)}$ and $q = q_0$ is a simple pole, simplifies the calculation

$$W = \frac{1}{2\pi i}2\pi i\sum_j R_j = R(q_0) = \frac{g(q_0)}{h'(q_0)} = \frac{t'(q_0)}{t'(q_0)} = 1$$

So to sum up,

$$W = \begin{cases} 0 & \text{No edge state exists} \\ 1 & \text{Edge state exists} \end{cases}$$

D Edge state results - Numerical analysis

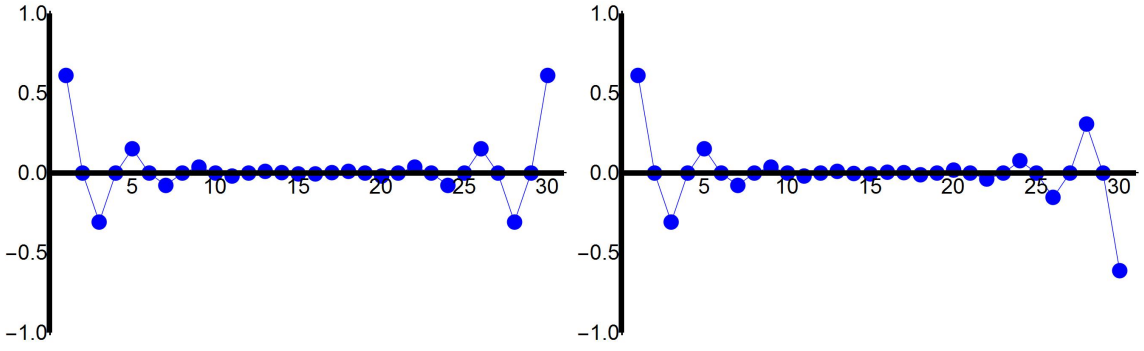

(a) Even state (b) Odd state

Figure 15: Plot of the numerical edge states as a functions of lattice site coordinate, where a) is the even state, and b) is the odd state. Here $t_1 = 0.5$ and $t_2 = 1$.

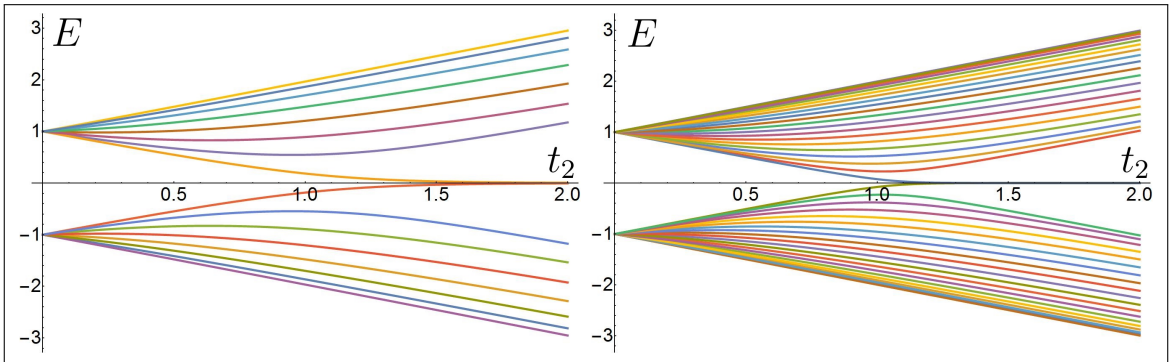

(a) $n = 16$ (b) $n = 40$

Figure 16: Plots of energy spectra as a function of t_2 where $t_1 = 1$ is held fixed. This shows the transition from a fully dimerized case, with no intercell hopping between unit cells, to the case of larger intercell compared to intracell hopping, i.e. $t_2 > t_1$ where we have edge states. Notice that for larger number of sites n, the hybridization becomes smaller, which can be seen as a smaller gap around $t_2 = t_1 = 1$.

E Comparison of bulk eigenstates - analytical and numerical

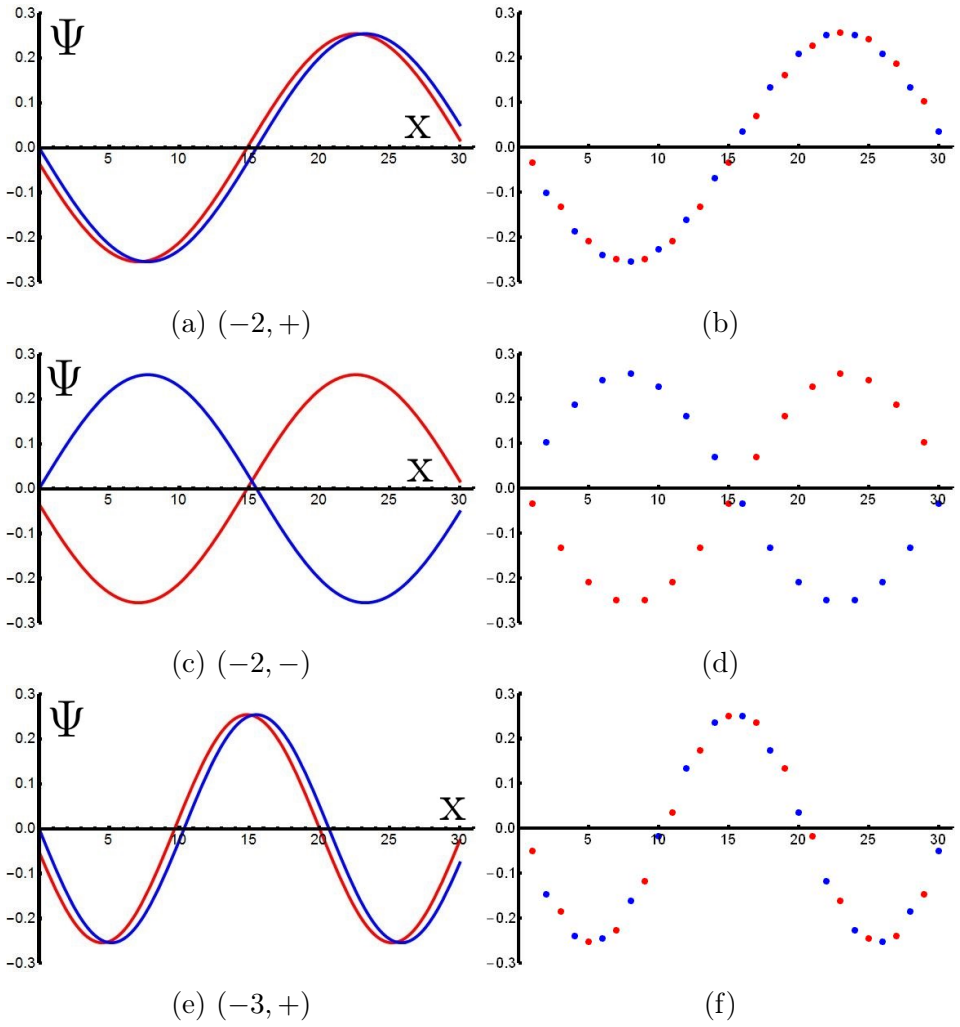

Figure 17: Comparison of analytical and numerical bulk eigenstates

F 1D model including on-site energy - Analytical calculation

To generalize the model in section 2, we can add on-site energies for the sublattices A and B. If we denote these by ϵ_a and ϵ_b the Hamiltonian from Eq. (4) reads

$$\mathcal{H}(k) = \begin{pmatrix} \epsilon_a & t^*(k) \\ t(k) & \epsilon_b \end{pmatrix} \tag{33}$$

But as we saw previously for the case without on-site potentials, the edge state is localized on only one sublattice. Therefore, adding the constant energy only shifts the energy of the edge state $E_0 = \epsilon_a$. This Hamiltonian can be written in a more symmetric expression as

$$\mathcal{H}(k) = \frac{\epsilon_a + \epsilon_b}{2} + \begin{pmatrix} h & t^*(k) \\ t(k) & -h \end{pmatrix} \Rightarrow \begin{pmatrix} h & t^*(k) \\ t(k) & -h \end{pmatrix}, \qquad h = \frac{\epsilon_a - \epsilon_b}{2} \tag{34}$$

Omitting the first term, being an offset that shifts the entire spectrum. The characteristic equation gives us the bulk energy spectrum of

$$E(k) = \pm\sqrt{h^2 + |t(k)|^2} \tag{35}$$

Which, compared to Eq. (6) is gapped for $h \neq 0$. The Hamiltonian in Eq. (34) can be cast in a form more generally used in condensed matter physics litterature, by using Pauli matrices. If we denote $\boldsymbol{\tau} = (\tau_x, \tau_y, \tau_z)$ working on the AB-sublattice space, where

$$\tau_x = \begin{pmatrix} 0 & 1 \\ 1 & 0 \end{pmatrix} \qquad \tau_y = \begin{pmatrix} 0 & -i \\ i & 0 \end{pmatrix} \qquad \tau_z = \begin{pmatrix} 1 & 0 \\ 0 & -1 \end{pmatrix}$$

Then the Hamiltonian simply becomes

$$\mathcal{H} = \boldsymbol{\tau} \cdot \mathbf{d}(k), \qquad \mathbf{d}(k) = (\mathrm{Re}[t(k)], \mathrm{Im}[t(k)], h) \tag{36}$$

The Shockley criterion now needs to be restated, and becomes more complex. As k sweeps the Brillouin zone, $d(k)$ traces a closed contour Γ in this 3D-space, and if the projection of Γ onto the xy-plane includes the origin, an edge state exists [3].

G Energyspectrum of the 3D Rashba spin orbit Hamiltonian

The energyspectrum of Eq. (20) can be found utilizing a clever trick, by squaring the Hamiltonian, and using that the Pauli matrices are involutory, i.e. their own inverse $\tau_i^2 = \sigma_i^2 = I$. Additionally it is used that the sublattice space and the spin space are decoupled, i.e. $\boldsymbol{\tau}$ does not act on $\boldsymbol{\sigma}$. In this case, if $\hat{A}$ and $\hat{B}$ are operators acting on different spaces, we use $\left(\hat{A} \otimes \hat{B}\right)\left(\hat{A}' \otimes \hat{B}'\right) = \hat{A}\hat{A}' \otimes \hat{B}\hat{B}'$, and one obtains

$$\begin{aligned} \mathcal{H}^2 &= \left(\tau_x^2 \otimes \sigma_0^2\right) \mathrm{Re}[t]^2 + \left(\tau_y^2 \otimes \sigma_0^2\right) \mathrm{Im}[t]^2 + \left(\tau_z^2 \otimes \sigma_x^2\right) \nu^2 p_y^2 + \left(\tau_z^2 \otimes \sigma_y^2\right) \nu^2 p_x^2 \\ &= I \otimes I(\mathrm{Re}[t]^2 + \mathrm{Im}[t]^2 + v^2(p_x^2 + p_y^2)) \end{aligned}$$

Where all cross-terms vanish due to the anti-commutation relations for the Pauli matrices $\{\sigma_i, \sigma_j\} = 2\delta_{ij} I$. The energyspectrum is then

$$E_\pm = \pm\sqrt{|t|^2 + \nu^2 |p|^2}$$

H 3D Bulk eigenfunctions for $\mathbf{p} \to 0$ - Rashba spin orbit case

The bulk eigenfunctions for the Rashba spin orbit case are in the limit $p \to 0$

$$\Psi^1_\pm \overset{\mathbf{p}\to 0}{=} \frac{1}{\sqrt{2}} \begin{pmatrix} \pm e^{-i\arg[t(k,\mathbf{p})]} \\ 0 \\ 1 \\ 0 \end{pmatrix}, \qquad \Psi^2_\pm \overset{\mathbf{p}\to 0}{=} \frac{1}{\sqrt{2}} \begin{pmatrix} 0 \\ \pm e^{-i\arg[t(k,\mathbf{p})]} \\ 0 \\ 1 \end{pmatrix}$$

If one substitutes k with $-k$ in these, the result is new eigenfunctions with the same energy. Additionally, if the two functions with negative energy (Ψ^A_- and Ψ^B_-) flips sign, the wavefunctions achieve the same form as in the 1D case (see Eq. (6)), and has equal probability on both sublattice planes A and B. $\Psi^1_\pm$ corresponds to spin up, and $\Psi^2_\pm$ corresponds to spin down.

I 3D surface state spinor

The 4-spinor $\psi^0_{p_y,p_z}$ can be found by looking at the SE, with a Hamiltonian given by Eq. (20) together with $E_0 = \pm\nu|p|$. Written out in real space, this gives the 4 recursion equations

$$\begin{aligned}
i\ \nu|p|e^{-i\varphi_p}\psi_{a\downarrow}(z) + t_1^*\psi_{b\uparrow}(z) + t_2^*\psi_{b\uparrow}(z-1) &= \pm\nu|p|\psi_{a\uparrow}(z) \\
-i\ \nu|p|e^{i\varphi_p}\psi_{a\uparrow}(z) + t_1^*\psi_{b\downarrow}(z) + t_2^*\psi_{b\downarrow}(z-1) &= \pm\nu|p|\psi_{a\downarrow}(z) \\
-i\ \nu|p|e^{-i\varphi_p}\psi_{b\downarrow}(z) + t_1\psi_{a\uparrow}(z) + t_2\psi_{a\uparrow}(z+1) &= \pm\nu|p|\psi_{b\uparrow}(z) \\
i\ \nu|p|e^{i\varphi_p}\psi_{b\uparrow}(z) + t_1\psi_{a\downarrow}(z) + t_2\psi_{a\uparrow}(z+1) &= \pm\nu|p|\psi_{b\downarrow}(z)
\end{aligned}$$

which can be cleaned up by using $\psi_{b\uparrow} = \psi_{b\downarrow} = 0$.

$$\begin{aligned}
i\ \nu|p|e^{-i\varphi_p}\psi_{a\downarrow}(z) &= \pm\nu|p|\psi_{a\uparrow}(z) \\
-i\ \nu|p|e^{i\varphi_p}\psi_{a\uparrow}(z) &= \pm\nu|p|\psi_{a\downarrow}(z) \\
t_1\psi_{a\uparrow}(z) + t_2\psi_{a\uparrow}(z+1) &= 0 \\
t_1\psi_{a\downarrow}(z) + t_2\psi_{a\uparrow}(z+1) &= 0
\end{aligned}$$

The last two equations are in accordance with the z-dependence found, and show that $\psi_{a\uparrow}(z)$ and $\psi_{a\downarrow}(z)$ differ only of a z-independent function, found by the first two equations by setting $\psi_{a\uparrow}(z) = 1$

$$\psi_{a\uparrow}(z) = 1 \qquad\qquad \psi_{a\downarrow}(z) = \mp i e^{i\varphi_p}$$

J Spin texture of surface states

To analyze the spin properties of the surface states, one can calculate the expectation values of the functions in Eq. 24 with the components of $\hat{\mathbf{S}} = \frac{\hbar}{2}\boldsymbol{\sigma}$. In this section I have calculated the expectation values of the spin part of the wavefunction in Eq. (24).

The z-dependent part of the wavefunction is already normalized and will not affect to expectation values. I consider only the first two entries in the spinor, corresponding to spin up and spin down on the sublattice A, i.e. $\psi_a = \frac{1}{\sqrt{2}}\begin{pmatrix}1\\ \mp ie^{i\varphi_p}\end{pmatrix}$. One then gets

$$\begin{aligned}\langle S_x\rangle &= \frac{\hbar}{2}\langle\psi_a|\sigma_x|\psi_a\rangle = \frac{\hbar}{4}\begin{pmatrix}1 & \pm ie^{-i\varphi_p}\end{pmatrix}\begin{pmatrix}0 & 1\\ 1 & 0\end{pmatrix}\begin{pmatrix}1\\ \mp ie^{i\varphi_p}\end{pmatrix}\\ &= \frac{\hbar}{2}\left(\frac{\pm e^{i\varphi_p} \mp e^{-i\varphi_p}}{2i}\right) = \pm\frac{\hbar}{2}\sin(\varphi_p)\end{aligned}$$

$$\begin{aligned}\langle S_y\rangle &= \frac{\hbar}{2}\langle\psi_a|\sigma_y|\psi_a\rangle = \frac{\hbar}{4}\begin{pmatrix}1 & \pm ie^{-i\varphi_p}\end{pmatrix}\begin{pmatrix}0 & -i\\ i & 0\end{pmatrix}\begin{pmatrix}1\\ \mp ie^{i\varphi_p}\end{pmatrix}\\ &= \frac{\hbar}{2}\left(\frac{\mp e^{i\varphi_p} \mp e^{-i\varphi_p}}{2}\right) = \mp\frac{\hbar}{2}\cos(\varphi_p)\end{aligned}$$

$$\begin{aligned}\langle S_z\rangle &= \frac{\hbar}{2}\langle\psi_a|\sigma_z|\psi_a\rangle = \frac{\hbar}{4}\begin{pmatrix}1 & \pm ie^{-i\varphi_p}\end{pmatrix}\begin{pmatrix}1 & 0\\ 0 & -1\end{pmatrix}\begin{pmatrix}1\\ \mp ie^{i\varphi_p}\end{pmatrix}\\ &= \frac{\hbar}{2}\left(\frac{1-1}{2}\right) = 0\end{aligned}$$

Where the $\pm$ refers to the sign of the energy. The spin is therefore locked perpendicular to the in-plane momentum, as shown in figure 10.

K Some properties of the Pauli spin matrices

The matrices are involutory

$$\sigma_x^2 = \sigma_y^2 = \sigma_z^2 = I$$

With commutation and anticommutation relations

$$[\sigma_i, \sigma_j] = 2i\epsilon_{ijk}\sigma_k \qquad \{\sigma_i, \sigma_j\} = 2\delta_{ij}I$$

Where ϵ_{ijk} is the Levi-Civita symbol, obeying

$$\epsilon_{ijk} = \begin{cases}+1 & \text{If (ijk) is an even permutation}\\ -1 & \text{If (ijk) is an odd permutation}\\ 0 & \text{Otherwise}\end{cases} \qquad \epsilon_{ijk}\epsilon_{imn} = \delta_{jm}\delta_{kn} - \delta_{jn}\delta_{km}$$

One can then derive the prodcut of two Pauli matrices as

$$\sigma_i\sigma_j = \frac{1}{2}\{\sigma_i, \sigma_j\} + \frac{1}{2}[\sigma_i, \sigma_j] = i\epsilon_{ijk}\sigma_k + \delta_{ij}I$$

And the product of 3 pauli matrices as

$$\begin{aligned}\sigma_l\sigma_i\sigma_j &= \sigma_l(i\epsilon_{ijk}\sigma_k + \delta_{ij}I) = i\epsilon_{ijk}\sigma_l\sigma_k + \delta_{ij}\sigma_l = i\epsilon_{ijk}(i\epsilon_{lkd}\sigma_d + \delta_{lk}I) + \delta_{ij}\sigma_l\\ &= -\epsilon_{ijk}\epsilon_{lkd}\sigma_d + i\epsilon_{ijl}I + \delta_{ij}\sigma_l = \epsilon_{kij}\epsilon_{kld}\sigma_d + i\epsilon_{ijl}I + \delta_{ij}\sigma_l\\ &= (\delta_{il}\delta_{jd} - \delta_{id}\delta_{jl})\sigma_d + i\epsilon_{ijl}I + \delta_{ij}\sigma_l\end{aligned} \tag{37}$$

After this rather tedious calculation, one can then conclude

$$\sigma_a\sigma_b\sigma_c = iI \qquad \sigma_a\sigma_a\sigma_c = \sigma_c \qquad \sigma_a\sigma_b\sigma_a = -\sigma_b$$

L Characteristics of the diamond lattice structure

The nearest-neighbour vectors, a_n are found to be

$$\begin{aligned} a_1 &= \frac{1}{2\sqrt{3}}\left(\sqrt{3}, 1, -2\sqrt{2}\right) \\ a_2 &= \frac{1}{2\sqrt{3}}\left(-\sqrt{3}, 1, -2\sqrt{2}\right) \\ a_3 &= \frac{1}{2\sqrt{3}}\left(0, -2, -2\sqrt{2}\right) \end{aligned}$$

And the in-plane time-reversal-invariant momenta are

$$\begin{aligned} \Gamma &= (0,0) \\ M_1 &= \left(-\pi, -\pi/\sqrt{3}\right) \\ M_2 &= \left(-\pi, \pi/\sqrt{3}\right) \\ M_3 &= \left(0, 2\pi/\sqrt{3}\right) \end{aligned}$$

The energy spectrum of the Hamiltonian in Eq. (25) can be found by writing $h(\mathbf{p})$ in the form using $\boldsymbol{\sigma} = (\sigma_x, \sigma_y, \sigma_z)$

$$\begin{aligned} h(\mathbf{p}) &= \frac{4\sqrt{2}}{3}\nu_{SO}\left(\boldsymbol{\sigma}\cdot[a_1\times a_2]\sin(\mathbf{p}\boldsymbol{\delta}_3) + \boldsymbol{\sigma}\cdot[a_2\times a_3]\sin(\mathbf{p}\boldsymbol{\delta}_1) + \boldsymbol{\sigma}\cdot[a_3\times a_1]\sin(\mathbf{p}\boldsymbol{\delta}_2)\right) \\ &= \boldsymbol{\sigma}\cdot\mathbf{d}(\mathbf{p}) \end{aligned}$$

$$\mathbf{d}(\mathbf{p}) = \frac{4\sqrt{2}}{3}\nu_{SO}\begin{pmatrix} \frac{1}{\sqrt{2}}\left(\sin(\mathbf{p}\boldsymbol{\delta}_2) - \sin(\mathbf{p}\boldsymbol{\delta}_1)\right) \\ \frac{1}{\sqrt{6}}\left(2\sin(\mathbf{p}\boldsymbol{\delta}_3) - \sin(\mathbf{p}\boldsymbol{\delta}_2) - \sin(\mathbf{p}\boldsymbol{\delta}_1)\right) \\ \frac{\sqrt{3}}{6}\left(\sin(\mathbf{p}\boldsymbol{\delta}_1) + \sin(\mathbf{p}\boldsymbol{\delta}_2) + \sin(\mathbf{p}\boldsymbol{\delta}_3)\right) \end{pmatrix}$$

In this form, the spectrum is

$$\begin{aligned} E_0(\mathbf{p})^2 = |\mathbf{d}(\mathbf{p})|^2 = \nu_{SO}^2\frac{32}{9}[\frac{3}{4}\left(\sin^2(\mathbf{p}\boldsymbol{\delta}_1) + \sin^2(\mathbf{p}\boldsymbol{\delta}_2) + \sin^2(\mathbf{p}\boldsymbol{\delta}_3)\right) \\ -\frac{1}{2}\left(\sin(\mathbf{p}\boldsymbol{\delta}_1)\sin(\mathbf{p}\boldsymbol{\delta}_2) + \sin(\mathbf{p}\boldsymbol{\delta}_2)\sin(\mathbf{p}\boldsymbol{\delta}_3) + \sin(\mathbf{p}\boldsymbol{\delta}_3)\sin(\mathbf{p}\boldsymbol{\delta}_1)\right)] \end{aligned}$$

M Time-reversal symmetry

The operation of time-reversal is representet by the operator Θ. For a real space Hamiltonian to be time-reversal invariant, it has to obey

$$[H, \Theta] = H\Theta - \Theta H = 0 \Leftrightarrow \Theta H \Theta^{-1} = H$$

For a spin-1/2 particle, the time-reversal operator obeys $\Theta^2 = -1$. This means that $\Theta^{-1} = -\Theta$, and Θ can be represented as[17]

$$\Theta = i\sigma_y K \qquad\qquad \Theta^{-1} = -i\sigma_y K \tag{38}$$

One can then ask the question: How does time-reversal act on physical observables like position, momentum and spin? To compute this, one can let the complex conjugation operator in Θ act on everything to the right, and use the porperties of the Pauli matrices (Appendix K)

$$\begin{aligned}
\Theta\mathbf{x}\Theta^{-1} &= i\sigma_y K x(-i\sigma_y K) = i\sigma_y x i(-\sigma_y)KK &&= \mathbf{x}\\
\Theta\mathbf{p}\Theta^{-1} &= i\sigma_y K(-i\hbar\partial_x)(-i\sigma_y K) = i\sigma_y i\hbar\partial_x i(-\sigma_y)KK = i\hbar\partial_x &&= -\mathbf{p}\\
\Theta\sigma_x\Theta^{-1} &= i\sigma_y K\sigma_x(-i\sigma_y K) = i\sigma_y\sigma_x i(-\sigma_y)KK = \sigma_y\sigma_x\sigma_y &&= -\sigma_x\\
\Theta\sigma_y\Theta^{-1} &= i\sigma_y K\sigma_y(-i\sigma_y K) = i\sigma_y(-\sigma_y)i(-\sigma_y)KK = -\sigma_y\sigma_y\sigma_y &&= -\sigma_y\\
\Theta\sigma_z\Theta^{-1} &= i\sigma_y K\sigma_z(-i\sigma_y K) = i\sigma_y\sigma_z i(-\sigma_y)KK = \sigma_y\sigma_z\sigma_y &&= -\sigma_z
\end{aligned} \tag{39}$$

So we see that time-reversal has the expected effect, i.e. even in the position $\mathbf{x}$, but odd in both linear momentum and spin. A Hamiltonian of the usual form ($\mathbf{p}^2$ for the kinetic part and $V = f(\mathbf{x})$ for the potential) is thus time-reversal invariant. For the Hamiltonian in Eq. (20), consisting of both sublattice space and spin space, the time-reversal operator is of the form $\Theta = i\tau_0 \otimes \sigma_y K$. The $\boldsymbol{\tau}$ part will be omitted since τ_0 preserves everything. For momentum space Hamiltonians, time-reversal symmetry implies

$$\Theta H(k)\Theta^{-1} = H(-k) \tag{40}$$

Which can be used to check the Rashba Spin-orbit Hamiltonian H_R,

$$\begin{aligned}
\Theta H_R(p_x, p_y)\Theta^{-1} &= i\sigma_y K\left[\nu(\sigma_x p_y - \sigma_y p_x)\right](-i\sigma_y K) = i\sigma_y\left[\nu(\sigma_x p_y + \sigma_y p_x)\right] i(-\sigma_y)KK\\
&= \nu(\sigma_y\sigma_x\sigma_y p_y + \sigma_y\sigma_y\sigma_y p_x) = \nu(-\sigma_x p_y + \sigma_y p_x) = H_R(-p_x, -p_y)
\end{aligned} \tag{41}$$

An important consequence of time-reversal symmetry is the Kramers degeneracy theorem, which states that for every eigenstate of a time-reversal invariant system, with spin-$\frac{1}{2}$, there is at least one other state with the same energy (called the time-reversed partner). This can be expressed by

$$H(k)|k\rangle = E(k)|k\rangle \qquad\qquad H(k)(\Theta|k\rangle) = \Theta(H(-k)|k\rangle) = E(-k)(\Theta|k\rangle)$$

Where Eq. (40) was used by exchanging $k \to -k$. This shows that time-reversal invariant momenta points (TRIM), where k and $-k$ can be related by a reciprocal lattice vector, are two-fold degenerate. Is there a term one can add to the Hamiltonian to break time-reversal symmetry, and thereby split this degeneracy? One can imagine that a term depending only on spin will break time-reversal symmetry, as the spin operators are odd under time-reversal. Such a term could be a Zeeman term,$H_Z = g^*\mu_B \boldsymbol{B}\cdot\boldsymbol{S}$, which stems from the fact that the intrinsic magnetic dipole moment of the electron couples to an external magnetic field $\boldsymbol{B}$.

N Periodic table of topological insulators and superconductors

Symmetry				d							
AZ	Θ	Ξ	Π	1	2	3	4	5	6	7	8
A	0	0	0	0	$\mathbb{Z}$	0	$\mathbb{Z}$	0	$\mathbb{Z}$	0	$\mathbb{Z}$
AIII	0	0	1	$\mathbb{Z}$	0	$\mathbb{Z}$	0	$\mathbb{Z}$	0	$\mathbb{Z}$	0
AI	1	0	0	0	0	0	$\mathbb{Z}$	0	$\mathbb{Z}_2$	$\mathbb{Z}_2$	$\mathbb{Z}$
BDI	1	1	1	$\mathbb{Z}$	0	0	0	$\mathbb{Z}$	0	$\mathbb{Z}_2$	$\mathbb{Z}_2$
D	0	1	0	$\mathbb{Z}_2$	$\mathbb{Z}$	0	0	0	$\mathbb{Z}$	0	$\mathbb{Z}_2$
DIII	-1	1	1	$\mathbb{Z}_2$	$\mathbb{Z}_2$	$\mathbb{Z}$	0	0	0	$\mathbb{Z}$	0
AII	-1	0	0	0	$\mathbb{Z}_2$	$\mathbb{Z}_2$	$\mathbb{Z}$	0	0	0	$\mathbb{Z}$
CII	-1	-1	1	$\mathbb{Z}$	0	$\mathbb{Z}_2$	$\mathbb{Z}_2$	$\mathbb{Z}$	0	0	0
C	0	-1	0	0	$\mathbb{Z}$	0	$\mathbb{Z}_2$	$\mathbb{Z}_2$	$\mathbb{Z}$	0	0
CI	1	-1	1	0	0	$\mathbb{Z}$	0	$\mathbb{Z}_2$	$\mathbb{Z}_2$	$\mathbb{Z}$	0

Figure 18: Periodic table of TI and TS, where the symmetry class can be determined by presence (or abscence) of time-reversal symmetry Θ, particle-hole symmetry Ξ and chiral symmetry $\Pi = \Xi\Theta$. The ± 1 is given by the value of Θ^2 or Ξ^2 and a 0 means no symmetry. After determining these, the dimensionality d can then show the topological characteristic. (Table is from [13]).

O The $\mathbb{Z}_2$ index

The difference between a material being in the Quantum spin Hall phase or the ordinary insulating phase is the existence of topologically protected boundary states, characterized by the $\mathbb{Z}_2$ topological invariant. A 3D topological insulator can be decribed by four $\mathbb{Z}_2$ numbers denoted by $(\nu_0; \nu_1, \nu_2, \nu_3)$, where ν_0 determines if the system is in a strong or weak topological phase. This section will describe how to determine these numbers, and is based on [9].

The recipe for determining $(\nu_0; \nu_1, \nu_2, \nu_3)$ is as follows. First one needs to solve the bulk momentum space Hamiltonian so that you can construct a unitary matrix given by

$$w_{ij}(k) = \langle u_i(-k)|\Theta|u_j(k)\rangle$$

Where Θ is the TR operator. Notice that we start with the bulk wavefunctions to compute the $\mathbb{Z}_2$ numbers (Bulk-boundary correspondance). Now, by using the TRIM points of the system, which can be expressed using the primitive reciprocal lattice vectors $(\mathbf{b_i})$ as $\Gamma_{i=n_1,n_2,n_3} = \frac{1}{2}(n_1\mathbf{b}_1 + n_2\mathbf{b}_2 + n_3\mathbf{b}_3)$ where $n_j = 0, 1$, the $w_{ij}(k)$ matrix can be used to evaluate a new entity δ

$$\delta_i = \frac{\sqrt{\det[w(\Gamma_i)]}}{\mathrm{Pf}[w(\Gamma_i)]} = \pm 1$$

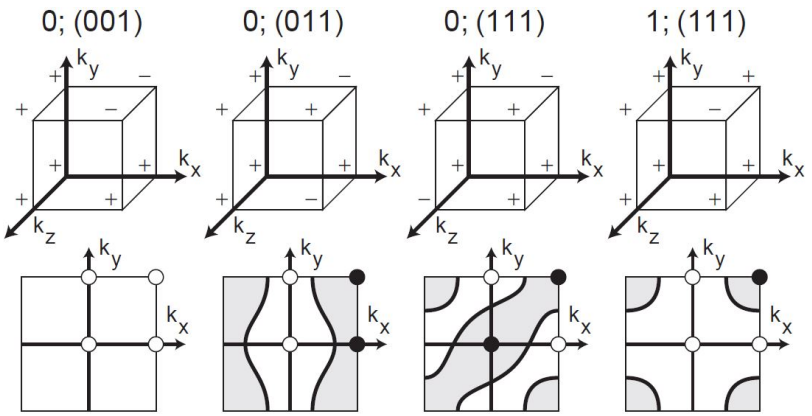

Figure 19: Picture of four different topological phases denoted by $(\nu_0;\nu_1,\nu_2,\nu_3)$. The first row depicts the value of δ_i at the various TRIM points Γ_i, while the second shows possible Fermi surfaces seen from the (001)-plane ($\hat{z}$-direction). The filled dots are Dirac cones included in the spectrum.[16] (The reason for the latter has to do with time-reversal polarization, which will not be discussed in this thesis). (Figure is from [9])

This can seem a bit frightening at first, but is actually fairly simple. In the denominator is the Pfaffian which is defined in the following way [9]. For an anti-symmetric matrix A the determinant can be written as the square of a polynomial $\det[A] = \mathrm{Pf}[A]^2$ which is precisely the Pfaffian. For example, an 2×2 matrix A with non-zero entries on the anti-diagonal has a Pfaffian that just picks out the A_{12} entry. After this rather technical procedure is completed, one can determine the topological invariants as

$$(-1)^{\nu_0} = \prod_{n_j=0,1} \delta_{n_1,n_2,n_3} \tag{42}$$

$$(-1)^{\nu_{i=1,2,3}} = \prod_{n_{j\neq i}=0,1;n_i=1} \delta_{n_1,n_2,n_3} \tag{43}$$

To clarify this let us look at an example. In figure 19 the reciprocal lattice of a cubic structure is shown, together with the value of δ at each of the 8 TRIM points. To find ν_0, according to Eq. (42) we just have to multiply δ at each point. The only case where this gives -1 is the last case, as the other three has an even amount of "-1's". Therefore only the last case has $\nu_0 = 1$. To find the other three $\mathbb{Z}_2$ numbers is a bit more tricky. For example, let us find ν_3. From Eq. (43) we just have to multiply all δ_i for all points with $n_3 = 1$. In all shown cases this gives $\nu_3 = 1$. The second row shows the possible Fermi surface arcs, and we observe that the only phase with an odd number of dirac cones is with $\nu_0 = 1$, i.e. the strong phase. Thus, we first determine the bulk wavefunctions, do some mathematical analysis, and end up with the four topological invariants $(\nu_0;\nu_1,\nu_2,\nu_3)$ that describe the topological phase.

P Symmetry class example

Let us determine the symmetry class of the spin-less Hamiltonian in the 1D case from Eq. (4). It has a TR symmetry given by $\Theta = K$, PH symmetry as $\Xi = \tau_z K$, and C

[9] https://en.wikipedia.org/wiki/Pfaffian

symmetry as $\Pi = \tau_z$ because of the following relations

$$\begin{aligned}
\mathcal{H}(k) &= \tau_x \mathrm{Re}[t(k)] + \tau_y \mathrm{Im}[t(k)] \\
\Theta\mathcal{H}(k)\Theta^{-1} &= K\left(\tau_x \mathrm{Re}[t(k)] + \tau_y \mathrm{Im}[t(k)]\right) K = \tau_x \mathrm{Re}[t(k)] - \tau_y \mathrm{Im}[t(k)] = \mathcal{H}(-k) \\
\Xi\mathcal{H}(k)\Xi^{-1} &= \tau_z K\left(\tau_x \mathrm{Re}[t(k)] + \tau_y \mathrm{Im}[t(k)]\right) \tau_z K = \tau_z\left(\tau_x \mathrm{Re}[t(k)] - \tau_y \mathrm{Im}[t(k)]\right) \tau_z \\
&= -\tau_x \mathrm{Re}[t(k)] + \tau_y \mathrm{Im}[t(k)] = -\mathcal{H}(-k) \\
\Pi\mathcal{H}(k)\Pi^{-1} &= \tau_z\left(\tau_x \mathrm{Re}[t(k)] + \tau_y \mathrm{Im}[t(k)]\right) \tau_z = -\tau_x \mathrm{Re}[t(k)] - \tau_y \mathrm{Im}[t(k)] = -\mathcal{H}(k)
\end{aligned} \tag{44}$$

In accordange with equations (29)-(31). Evaluating the square of these, $\Theta^2 = KK = 1$, $\Xi^2 = \tau_z K \tau_z K = 1$ and $\Pi^2 = \tau_z^2 = 1$, where 1 means the identity, and looking at Appendix N, shows that this belongs to class BDI. Thus, it has a $\mathbb{Z}$ topological classification, which is the winding number discussed in section 2.5. Not all integers can be obtained, but this is due to the specifics of the system, i.e. there can only be one edge-state per edge.

Q Miller indices

In section 4 the concept of a weak TI is introduced, and the corresponding topological invariants (ν_1, ν_2, ν_3) was related to a reciprocal lattice vector $G_\nu = \sum_i \nu_i \mathbf{b}_i$ where $\mathbf{b}_i$ are the primitive reciprocal lattice vectors of the system. (ν_1, ν_2, ν_3) can then be interpreted as Miller indices for a surface that determines the direction of stacked 2D QSH system[9]. So what are these Miller indices?

Miller indices is also known as the index system for crystal planes[5], and are denoted by integers (hkl). To specify a crystal plane, you need 3 points (that are not on a straight line), and it turns out to be advantageous to use the reciprocal lattice vectors to decribe surfaces. It is done using the following rules

- Find the intercepts of the plane with the axes given by $\mathbf{a_1}, \mathbf{a_2}, \mathbf{a_3}$.
- Take the reciprocals of the numbers
- Reduce to integers having the same ratio

For example, if a plane intersects at $x = 4$, $y = 2$, $z = 2$, the index of the plane would be $(422) \to (\frac{1}{4}\frac{1}{2}\frac{1}{2}) \to (122)$. In figure 20 there a a couple of examples of surfaces, with their corresponding Miller indices. In cubic crystals a vector with coordinates [hkl] is a normal vector to the plane (hkl), but this is not true for other crystal structures.

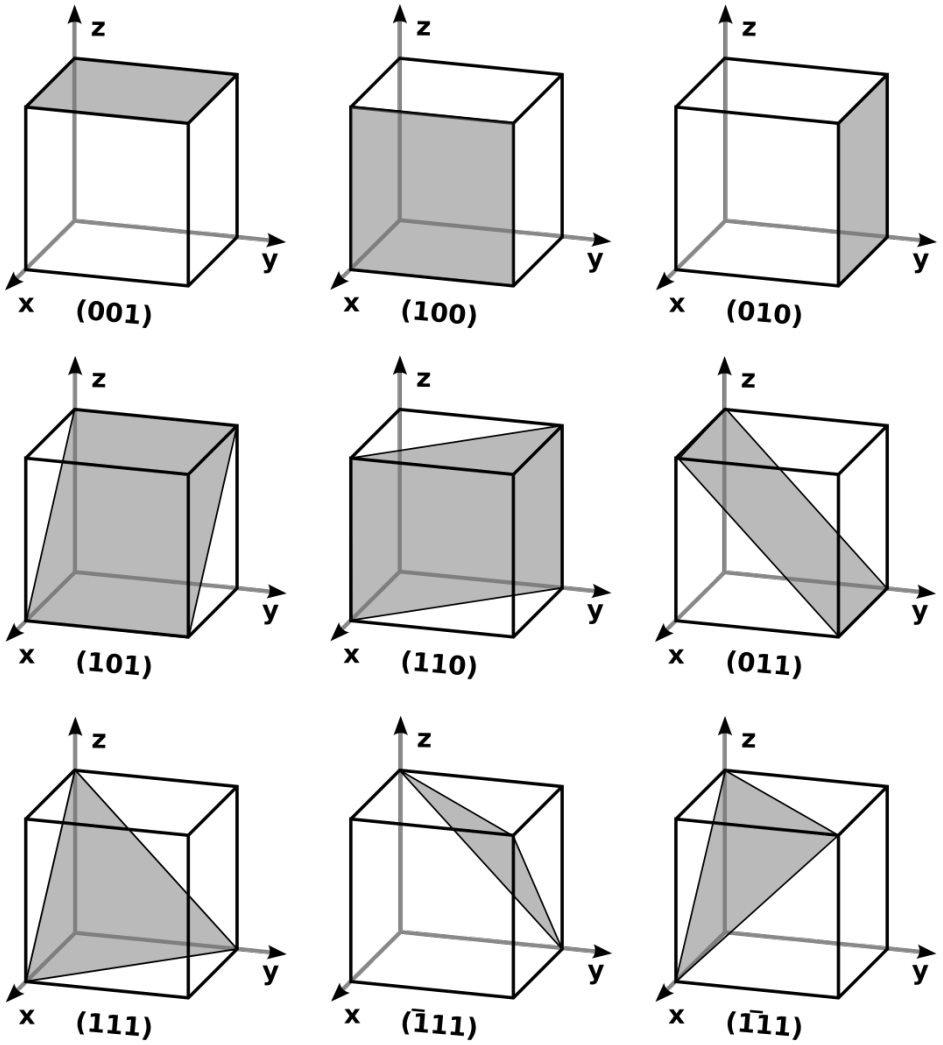

Figure 20: Examples of crystal surface planes and their associated Miller indices.